the tissue is not influenced by blood flow. This method has been used to study glucose metabolism, neuroreceptor assays and neurotransmitter release in animal brain tissues (Matsumura et al., 1995; Murata et al., 1996; Sasaki et al., 2002a,b).

Surgery has been recognized as an effective treatment for certain epileptic patients, such as those with medically intractable temporal lobe epilepsy (TLE) (Cascino et al., 2004). Presurgical imaging using PET, single photon emission tomography, and magnetic resonance imaging (MRI) is used to assess the feasibility of surgery and to decide the scale of excision in regions with spike activity (Casse et al., 2002; Matheja et al., 2000). The brain regions estimated to have low glucose metabolism by 2-[^{18}F]fluoro-2-deoxy-D-glucose (FDG)-PET are diagnosed as the excision extent including epileptogenic foci (Casse et al., 2002). Noninvasive molecular-imaging techniques such as PET have potential roles in disease diagnosis and therapy, but diagnosis as in the case of epilepsy is influenced by several factors and problems, for example, biodegradation of the radioligand, influence of blood flow on radioligand delivery, and limited spatial resolution. In order to confirm PET diagnosis, glucose metabolism in living human brain tissue in vitro was compared with preoperative FDG-PET findings using bioradiography with FDG in brain slices obtained at operation from patients with intractable epilepsy.

Results

The experimental flowchart is shown in Fig. 1. All seven patients underwent excisions of pathological lesions and the area with epileptogenecity surrounding them identified by presurgical FDG-PET, MRI, and intraoperative cortical electroencephalography (EcoG). In all cases, a significant amelioration of seizures was achieved by surgery. This indicated that the epileptic foci and the pathological brain surrounding them were precisely detected and resected. In all the patients, cortical gyri sampled for slice analysis were not the epileptic foci themselves but the gyri surrounding the focus from where an abnormal EcoG pattern was recorded. Though three of seven patients harbored low-grade gliomas, the proliferation rate of tumor cells determined from the labeling rate with a monoclonal antibody (MIB-1) against nuclear antigen Ki-67 (Ki labeling index) was very low (<1% in two and 5% in one) and therefore none of them were invasive tumors. No tumor cells were identified in the sampled gyri of three of tumor patients. Therefore, we concluded that the sampled cortical gyri used for autoradiographical analysis was the cortex outside the main lesions but influenced by chronic epileptic conditions (Table 1).

As shown in Table 2 and Fig. 5, FDG uptake in the sampled gyri was lower than that in the contralateral gyri or cere-
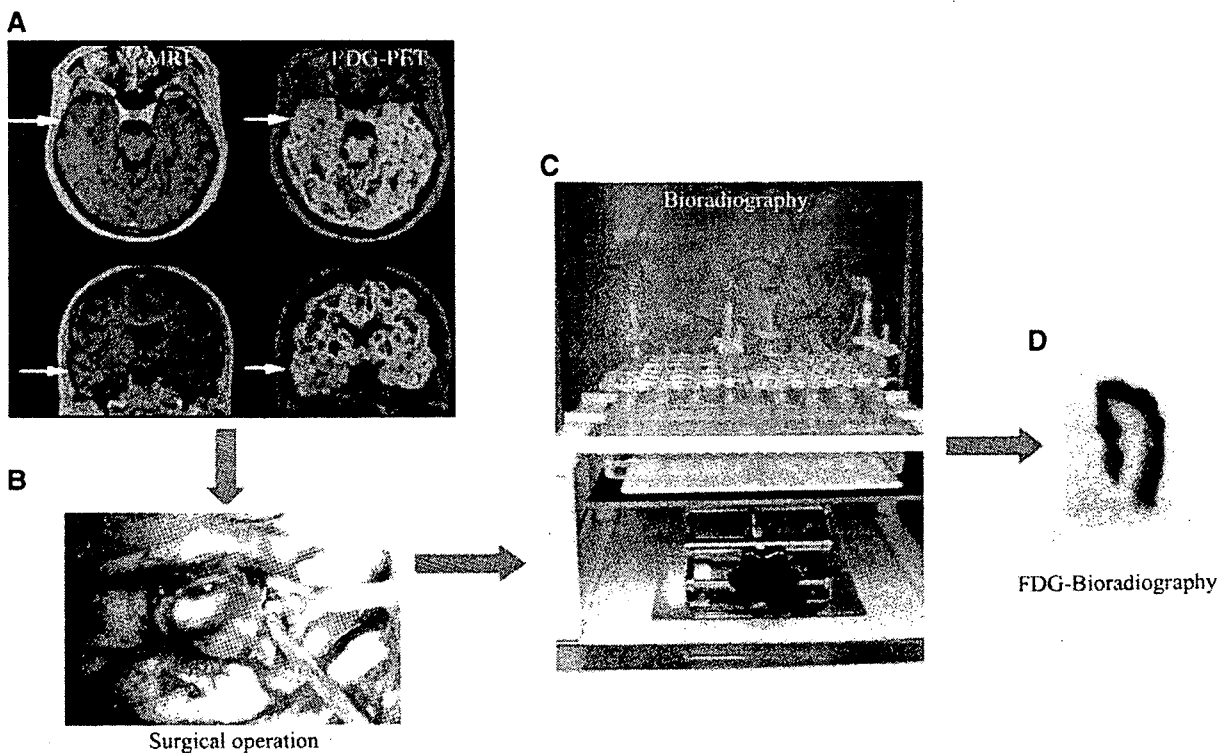
Fig. 1 – Flowchart for bioradiography in human brain slices. (A) The presurgical evaluation of patients with medically intractable epilepsy was performed with FDG-PET co-registered to MRI. FDG-PET showed hypo-glucose metabolism in the right temporal cortex (arrow). (B) Epileptic foci and the epileptogenic cortical gyrus surrounding them were surgically excised (arrow). The former was subjected to routine pathological analysis and the latter to bioradiographical analysis. (C) Bioradiography for analysis in vitro using human and animal brain slices. (D) FDG bioradiographic image of an excised human brain slice.

Table 1 – Patient characteristics					
Case number	Age (years) and sex	Age at seizure onset (years)	Side of lesions	Pathology (Ki labeling index)	Surgical outcome (follow-up periods)
1	35, Female	26	Right	Dysembryoplastic neuroepithelial tumor (<1%)	Free (4 years)
2	25, Male	20	Left	Cavernous angioma	Free (4 years)
3	48, Male	20	Left	Pleomorphic xanthoastrocytoma (5%)	Free (4 years)
4	27, Female	13	Left	Hippocampal sclerosis	Free (4 years)
5	26, Female	12	Left	Hippocampal sclerosis	Free (3 years)
6	25, Female	15	Left	Hippocampal sclerosis	Free (3 years)
7	19, Female	17	Left	Low grade astrocytoma (<1%)	1–2/year (4 years)

bellum. This result also indicated that all the sampled gyri were pathological cerebral cortex to different degrees among patients. Typical uptake patterns of FDG in human and rat brain slices are shown in Figs. 2 and 3. The uptake in human and rat brain under control and high K^+ conditions increased continuously up to 250 min. The white matter showed slightly greater uptake than the gray matter under the control condition (Figs. 2 and 3). The uptake of FDG in human gray matter was significantly enhanced by a neuro-stimulant, high K^+ ($P=0.0049$ from control gray matter with an outlier and $P=0.0050$ without an outlier), whereas that in the white matter was not enhanced (Fig. 4). The uptake in rat gray matter was also enhanced by high K^+ ($P=0.0051$ from control gray matter). The average rate of uptake per pixel per minute in high K^+-treated human (including outlier) and rat brain was increased 7.0- and 7.6-fold compared to the control level, respectively (Fig. 4). The uptake in human gray matter under both control and high K^+ conditions did not differ significantly from that in rat (Fig. 4). However, significant differences between rat and human tissues were found in variance under the control condition ($P=0.0001$) and the control/high K^+ ratio ($P=0.0005$).

The relationship between FDG uptake in PET and bioradiography is shown in Fig. 5. The outlier was contained in the human data (arrow in Fig. 5). The relationship was analyzed between FDG-PET and FDG bioradiographic data with an outlier (7 patients) and without (6 patients). The rates of uptake in gray matter of brain slices under the control condition showed an inverse correlation with those seen in PET, evaluated as the sampled and contralateral gyri (SG/CG)

ratio ($r=0.936$, $P=0.0007$ with an outlier and $r=0.814$, $P=0.0494$ without) and the sampled gyri and cerebellar cortex (SG/CB) ratio ($r=0.788$, $P=0.0330$ with an outlier and $r=0.896$, $P=0.0156$ without) (Fig. 5). In contrast, it showed a weak positive correlation with PET under the high K^+ condition, but this was not statistically significant. The rates of uptake in gray matter of brain slices, expressed as the high K^+/control ratio, correlated with those seen in PET, evaluated as the SG/CG ratio ($r=0.844$, $P=0.0134$ with an outlier and $r=0.691$, not significant without) and the SG/CB ratio ($r=0.904$, $P=0.0028$ with an outlier and $r=0.828$, $P=0.0417$ without) (Fig. 5).

Discussion

We have examined the bioradiographic images of FDG in human and rat brain slices under the control and high K^+ conditions and compared them with FDG-PET. Normal human brain cannot be used for in vitro studies as a reference for ethical reasons. We speculated that brain tissue from animals with well-controlled breeding could be a substitute for human brain tissues, and the uptake of FDG in animal tissues would show little variance because there is no morbidity. On the other hand, the variance in epileptic brain tissue shows a large degree of variance, depending on the progress of the epilepsy. Indeed, significant differences in variance between rat and human tissues were found in the uptake of FDG under the control condition and in which expressed the high K^+/control ratio.

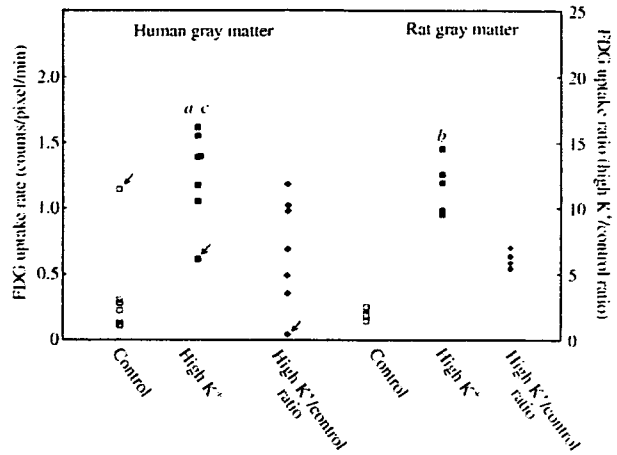| Table 2 – Details of the PET and bioradiography data for seven patients						
Case number	PET[a]		Bioradiography[b]			Time interval between PET and bioradiography
	SG/CG ratio	SG/CB ratio	Control	High K^+	High K^+/control ratio	
1	0.9593	0.8741	1.43	14.23	9.95	<1 month
2	0.8273	0.7895	2.92	10.75	3.68	1 month
3	0.7409	0.7853	3.16	15.75	4.98	<1 month
4	0.8746	0.9029	1.19	14.23	11.96	7 years
5	0.8868	0.8545	2.34	16.47	7.04	3 months
6	0.9193	0.9918	1.16	12.10	10.43	2 months
7	0.5479	0.7063	11.55	6.35	0.55	<1 month

[a] FDG uptake in PET was calculated as the ratio between the sampled and contralateral gyrus (SG/CG) or the sampled gyrus and cerebellum (Sg/CB).
[b] FDG bioradiographic uptake in gray matter of the brain slices was expressed as the rate of uptake per pixel per minute (counts/pixel/min) in control medium, that in high K^+ medium and the uptake ratio between high K^+/control media.
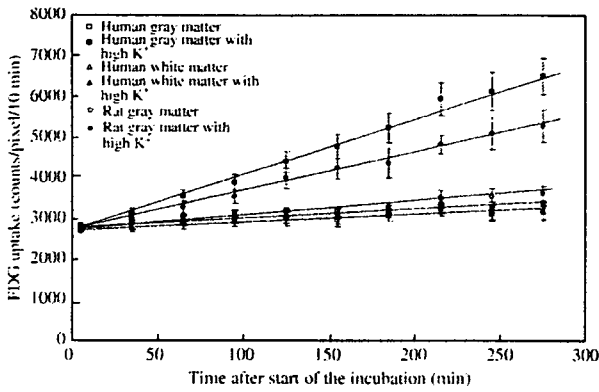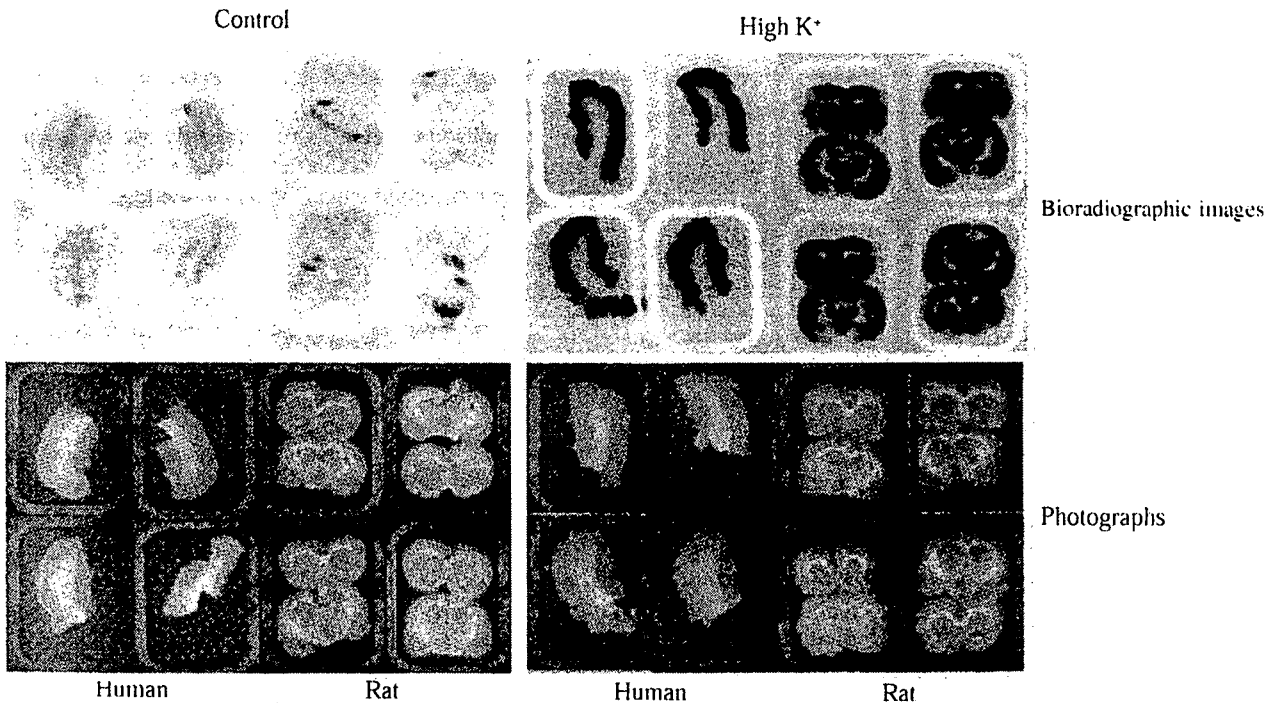
Fig. 2 - Time-courses of FDG uptake in human and rat brain slices (control and high K⁺ treatment).

Fig. 4 - Rate of FDG uptake in control and high K⁺-treated human and rat brain slices. The bioradiographic uptake in tissue slices was expressed as the rate of uptake per pixel per minute (counts/pixel/min) in control medium (left), that in high K⁺ medium (middle), and the uptake ratio between high K⁺/control media (right). The values are the mean ± SD for 7 patients and 6 rats. Statistical significance was determined by the Wilcoxon/Kruskal-Wallis test for differences of data with an outlier (arrow) ($^a P = 0.0049$ from control human gray matter and $^b P = 0.0051$ from control rat gray matter) and without an outlier ($^c P = 0.0050$ from control human gray matter). Significant differences in variance between rat and human tissues were found in FDG uptake under the control condition ($P = 0.0001$) and the control/high K⁺ ratio ($P = 0.0005$).
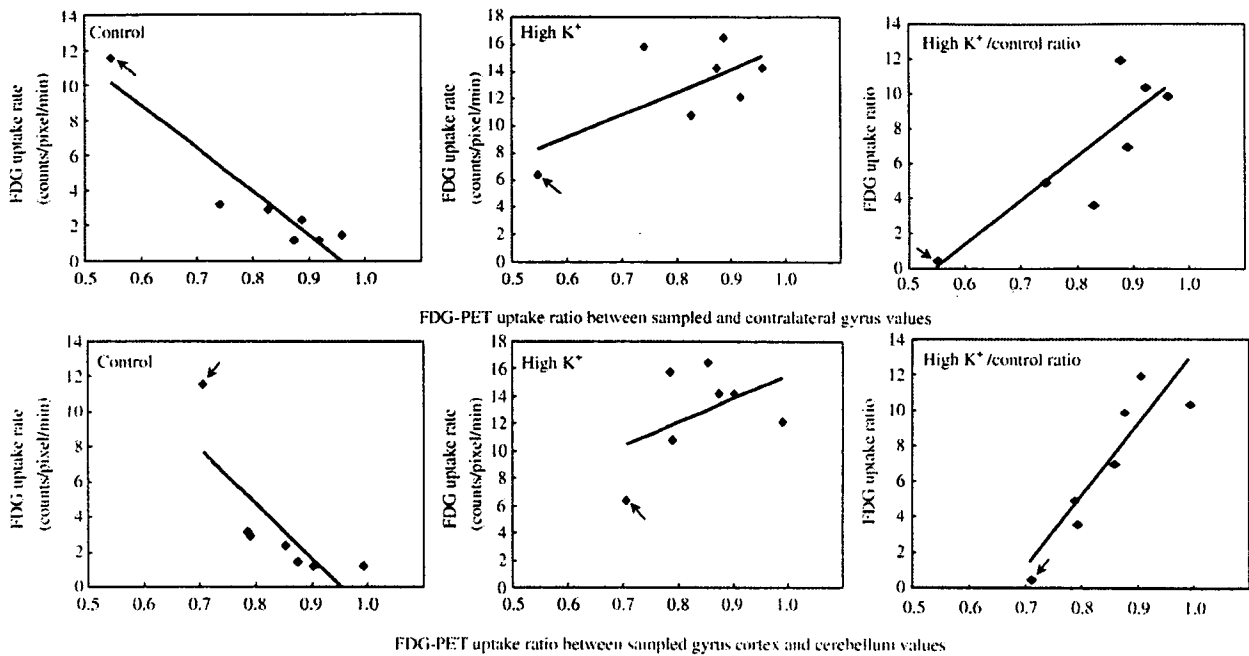
FDG uptake in the gray matter was significantly enhanced (seven times the control) by high K⁺, whereas that in the white matter was not enhanced compared to the control condition. In the control condition, FDG uptake was slightly lower in gray matter than white matter (Figs. 2–4). A higher metabolic rate of FDG in gray matter than white matter was observed in PET studies, but the ratio of gray/white matter FDG metabolic rates was only about 2 (Huang et al., 1980; Reivich et al., 1985). The limited spatial resolution of PET introduces a partial volume effect, thereby causing an admixture of FDG metabolic rates in gray and white matter regions, and this might account for the discrepancy. Another factor could be the K⁺ concentration. The resting extracellular K⁺ concentration in the brain in vivo

Fig. 3 - Bioradiographic images at the 9th exposure (240–250 min) and photographs of control and high K⁺-treated human and rat brain slices.

FDG-PET uptake ratio between sampled and contralateral gyrus values

FDG-PET uptake ratio between sampled gyrus cortex and cerebellum values

Fig. 5 – Relationship between FDG uptake in PET and bioradiography. FDG uptake in PET was calculated as the ratio between that in the sampled and contralateral gyrus (SG/CG) (upper) or the sampled gyrus and cerebellar cortex (SG/CB) (lower). FDG bioradiographic uptake in gray matter of the brain slices was expressed as the rate of uptake per pixel per minute (counts/pixel/min) in control medium (left), that in high K$^+$ medium (middle), and the uptake ratio between high K$^+$/control media (right). The values compared favorably with SG/CG and SG/CB uptake ratios obtained by PET. The uptake rates of FDG in brain slices under the control condition showed an inverse correlation with those seen in PET, evaluated as the SG/CG ratio (r=0.936, P=0.0007 with an outlier and r=0.814, P=0.0494 without) and the SG/CB ratio (r=0.788, P=0.0330 with an outlier and r=0.896, P=0.0156 without). The uptake rates of FDG, expressed as the high K$^+$/control ratio, correlated with those seen in PET, evaluated as the SG/CG ratio (r=0.844, P=0.0134 with an outlier and r=0.691, not significant without) and the SG/CB ratio (r=0.904, P=0.0028 with an outlier and r=0.828, P=0.0417 without). An arrow indicates the outlier.

is normally ~3 mM and increases to 12 mM during neuronal activation. It rises as high as 50–80 mM in seizures (Somjen, 1975). In our study, the FDG-PET images were acquired in the interictal, not ictal, period. The K$^+$ concentration (50 mM) in the present in vitro study might correspond to the ictal concentration in vivo. This concentration might be higher than that in the interictal period. In the central nervous system, gray matter is constituted from perikaryons, unmyelinated fibers, protoplasmic astrocytes, and microglia, and white matter from myelinated fibers, oligodendrocytes, fibrous astrocytes and microglia (Graham and Lantos, 2002). The greater metabolic rate of glucose and higher sensitivity to high K$^+$ in gray matter is explained by the high density of neurons, as well as the sensitivity of neurons to high K$^+$ and the insensitivity of neuroglia (Takahashi et al., 1995; Sokoloff et al., 1996; Sokoloff, 1999; Honegger and Pardo, 1999).

Low glucose metabolism in epileptic brain regions including foci has been detected by FDG-PET (Huang et al., 1980; Casse et al., 2002). In all seven patients who underwent excisions of epileptogenic foci and surrounding them identified by presurgical FDG-PET, the uptake of FDG was lower in the sampled gyrus than in the contralateral gyrus and cerebellum (Table 2 and Fig. 5). These uptake ratios for FDG-PET, correlated well with the uptake rates in gray matter of the

human brain slices expressed as a high K$^+$/control ratio (Fig. 5, right), and weakly correlated with those in brain slices under the high K$^+$ condition but not significantly (Fig. 5, middle). However, the uptake rates of FDG in gray matter of the human brain slices under the control condition showed an inverse correlation with those seen in PET (Fig. 5, left). These results indicated that normality in response ability to a neuro-stimulant such as high K$^+$ relates to FDG uptake in epileptic brain regions including foci and surrounding them by PET. The working brain in vivo responds to stimulants from outside of the brain via nerve fibers, but the number of input signals is restricted partially in brain slices in vitro. Glucose metabolism in brain slices under the control culture condition might be too silent compared to that in the working brain. Therefore, this condition could not reflect FDG uptake in vivo. Even in the control condition, the brain slices which had shown low FDG uptake in vivo, had high uptake rates (Fig. 5, left). Such high glucose metabolism might indicate an abnormal response to stimuli in epileptic brain regions. Brain slices from one of the seven patients (arrow in Figs. 4 and 5) showed rather abnormal glucose metabolism. In this case, the specimen had been taken from epileptic tissue surrounding a low-grade astrocytoma, and pathological examination demonstrated gliosis without either normal cortical structures or tumor cells. Brain slices of this patient showed high glucose metabolism even

in the control medium, but poor sensitivity to high K⁺. This phenomenon can be explained in terms of the properties of glial cells.

In the brain of an epileptic patient, neuronal death and gliosis progress as a result of repeated excessive excitement of neurons (Cohen-Gadol et al., 2006; Velisek and Moshe, 2003). In Alzheimer's brain, the area of hypo-glucose metabolism in PET correlated with that of neuronal loss and the proliferation of glia (McGeer et al., 1986; Minoshima et al., 1999). In a presurgical evaluation of temporal lobe epilepsy, both FDG and [¹¹C] flumazenil PET reliably indicated the epileptogenic temporal lobe. Decreased [¹¹C]flumazenil binding simply reflects a loss of neurons expressing the benzodiazepine-GABA receptor, but the area of hypometabolism in FDG-PET was more extensive than the areas of the epileptogenic temporal lobe and the decreased [¹¹C]flumazenil binding (Debets et al., 1997). The neuroglia is known to be insensitive to extracellular K⁺ (Takahashi et al., 1995; Sokoloff et al., 1996; Sokoloff, 1999; Honegger and Pardo, 1999). These results indicate that neuronal loss and gliosis in epileptogenic brain regions could be one reason for the hypo-glucose metabolism in PET.

As another explanation, impaired glutamatergic signaling is considered a mechanism of the hypo-glucose metabolism seen in FDG-PET. Glutamate is the principal excitatory transmitter within the vertebrate nervous system (Meldrum, 2000). During seizures, the glutamate concentration in epileptogenic brain regions increases to neurotoxic levels (During and Spencer, 1993). The increase in glutamate or its degradation product glutamine continues even after the seizures (Fazekas et al., 1995). Increased glutamate in epileptogenic brain regions is hypothesized to be due to slow rates of glutamate–glutamine cycling (Petroff et al., 2002). However, another report showed that glucose metabolism and glutamate cycling in epileptogenic brain using FDG-PET and 1H magnetic resonance spectroscopy (Pfund et al., 2000). The decrease in glucose metabolism and glutamate (NMDA) receptor demonstrated using FDG-PET, and [¹¹C]ketamine also indicates that glutamatergic signal transduction activity could be decreased with hypo-glucose metabolism (Kumlien et al., 1999).

Glutamatergic synaptic transduction is highly energy requiring. Cortical glucose oxidation coupled to glutamatergic synaptic activity accounts for over 80% of total glucose oxidation (Sibson et al., 1998). However, if glutamic acid-related signal transduction is depressed by repeated seizures, it could be one of the reasons for hypo-glucose metabolism in PET. The release of neurotransmitters including glutamate is enhanced by high K⁺, a depolarizing agent (Zheng et al., 2000). The depressing of glutamate-related signal transduction in epileptogenic brain regions could cause low sensitivity of FDG uptake to high K⁺ and the low high K⁺/control uptake ratio. Therefore, the progression of neuronal loss including glutamatergic neuron and gliosis in the epileptogenic brain could also cause the poor response of FDG uptake to high K⁺ and the low high K⁺/control uptake ratio. We consider that the abnormal response to a neuro-stimulant such as high K⁺ underlying reduced transduction and/or neuronal loss and gliosis relates to hypo-glucose metabolism in epileptogenic brain regions by PET.

The glucose transporter (Glut1) has been analyzed and quantified in brain tissues from patients undergoing surgery for seizures. Blood–brain barrier glucose transporter1 Glut1 has been suggested as up-regulated in seizures (Cornford et al., 1994). Endothelial Glut1 demonstrated increased quantities in the extravascular regions in which more EEG spiking activity had been demonstrated in interictal seizure resections (Cornford et al., 1998). These observations seem to conflict with the hypo-glucose metabolism seen in FDG-PET. However, they can be explained by the result that the FDG uptake in brain slices under the control condition showed an inverse correlation with that seen on PET. Thus the neural activity in brain slices under the control condition is less silent than that in the working brain as discussed above. In such conditions in vitro, FDG uptake could reflect Glut1 glucose transporter activity in the brain. However, FDG uptake in the epileptic brain could be defined by the response to neuro-stimulant rather than Glut1 glucose transporter activity. We speculated that the sensitivity is high under the control condition to detect the seriousness of epilepsy because it has low basement FDG uptake levels. The variance of FDG uptake in epileptic brain tissue under the high K⁺ condition did not differ from that in the rat as a reference. This finding means that the sensitivity for the detection of epilepsy is low in FDG bioradiography under the high K⁺ condition. The K⁺ concentration (50 mM) in the present in vitro study might correspond to the ictal concentration in vivo as described above. This high K⁺ concentration might be a case of low sensitivity on detection of epilepsy and poor correlation between FDG uptake in epileptic brain tissue under the high K⁺ condition and that in PET.

In this study, FDG uptake in vitro expressed as a high K⁺/control ratio was strongly correlated with FDG uptake in PET expressed as SG/CG and SG/CB values (Fig. 5, right). The reason is that FDG uptake in brain slices under the control condition irreversibly correlated with those in FDG-PET. To obtain the absolute values of PET data are sometimes technically difficult. In this study, we used relative values as an approximate substitute. FDG uptake in epileptogenic brain region was expressed as SG/CG and SG/CB values. FDG uptake expressed as ipsilateral to contralateral values is useful to predict outcome. Eighty six percent of TLE patients showed unilateral temporal lobe hypometabolism (UTH) and of UTH predicted a good outcome in 82% of cases. Fifty percent of patients with bitemporal hypometabolism had independent bilateral foci, and of those who proceeded to surgery only 50% had a good result (Casse et al., 2002). If we can obtain the absolute FDG uptake value in epileptogenic brain region, it would show the irreversible relation with the seriousness of epileptogenic brain. Moreover, the order of magnitude in FDG uptake in epileptogenic brain region must agree with that in the brain slices under the high K⁺ condition. Indeed, in all seven patients who underwent excisions of epileptogenic foci and the area surrounding them identified by presurgical FDG-PET, FDG uptake in the sampled gyrus was lower than that in the contralateral gyrus and cerebellum (Table 2 and Fig. 5). FDG uptake rates in brain slices expressed as the high K⁺/control ratio is a good indicator of the progress of epilepsy. However, it is based upon the sensitivity of morbid FDG uptake in brain slices which is high under the control condition.

Brain slices are in a sense intermediate between *in vitro* cell culture and *in vivo* studies, because the neural network and cell-to-cell communication are partially maintained in slices. In this study, the part of the brain examined in bioradiography was identical with that visualized by PET, and a comparison of *in vitro* with *in vivo* results is possible. Moreover, metabolism and physiological function in living human tissue can be compared with those in animal tissues in the same apparatus under the same conditions (Fig. 3), allowing us to evaluate the relevance of animal findings to humans.

An *in vivo* diagnosis based on PET, is influenced by several factors, for example, bio-degradation of the radioligand, influence of blood flow on radioligand delivery, and a limited spatial resolution (Reivich et al., 1985). Our experimental system could be useful for validating a PET-based diagnosis. In addition, various coefficients and factors, for example, the Lumped constant (Huang et al., 1980; Reivich et al., 1985), are needed for PET image processing, and their values are not always based on substantial evidence. Our system would be helpful to obtain reliable experimental values of coefficients and factors.

In order to validate diagnosis based on PET, a novel autoradiographic examination "bioradiography" was carried out in human neocortical brain slices obtained at operation from patients with intractable epilepsy who had received an FDG-PET examination preoperatively. The glucose metabolism detected in brain slices by bioradiography matched that observed by PET. Our experimental system could provide useful information for the interpretation of PET data in epileptics. It also provided a theoretical basis in performing experiments using human brain tissue that can be used to examine the pharmacological manipulation using human brain slices.

Experimental procedures

In vivo study

We studied seven patients (2 men and 5 women, mean age 29.3±9.5 years) with medically intractable TLE. Patient characteristics are listed in Table 1. Magnetic resonance imaging studies were performed using a 1.5-T superconducting system with a maximal gradient capacity of 25 mT/m (Magnetom Vision; Siemens, Erlangen, Germany) and a circularly polarized head coil. PET measurements were carried out by measuring the equilibrated radioactivity 45 min after i.v. injection of FDG (150 MBq) using a PET scanner (Headtome V, Shimadzu, Kyoto, Japan). The transmission data were acquired for each patient with a rotating germanium-68 rod source for attenuation correction. The regional uptake of FDG was expressed as a standardized uptake value (SUV) (tissue activity/ml)/(injected radioisotope activity/body weight (g)). Image analysis was carried out using a medical image processing software Dr. View (Asahi Kasei Joho System Co. Ltd., Tokyo, Japan) working on a personal computer. PET data of each patient were co-registered to their own MRI using the automatic multimodality image registration (AMIR) software (Ardekani et al., 1995). Cortical

gyri sampled for brain slice study were identified on MRI and the regions of interest (ROIs) were manually placed on them. The ROIs were also placed on the cortical gyri contralateral to the sampled area and on the cerebellar cortex. The regional FDG uptake (SUV) of these ROIs was obtained from PET images co-registered to MRI. The ratios between the sampled and the SG/CG and between the SG/CB were calculated. All seven patients underwent excisions of epileptogenic foci and the surrounding neocortex with spike activity in intraoperative recordings.

In vitro study

Preparation of brain slices

Brain regions determined to have epileptogenecity were excised and were subjected to routine pathological examination and bioradiographical assay. For the latter, surgical specimen were rapidly transferred into oxygenated ice-cold Krebs–Ringer medium (124 mM NaCl, 5 mM KCl, 2 mM $CaCl_2$, 1 mM $MgCl_2$, 1.2 mM KH_2PO_4, 26 mM $NaHCO_3$ and 10 mM glucose). Then they were sectioned at 300 μm with a tissue cutter (Microslicer DTK-3000W; Dosaka EM, Kyoto, Japan) and slices were transferred into oxygenated ice-cold Krebs–Ringer medium described previously (Sasaki et al., 2002a,b). Male Wistar rats (Tokyo Jikken Dohbutsu Co. Ltd., Japan), 2 months old, were sacrificed by decapitation under light diethyl ether anesthesia. The brain was rapidly removed and placed on a tissue cutter, and coronal slices were sectioned as described above. Sectioning of all human and rat brain tissues was started within 5 min of the brain's removal. Parts of the surgical specimens were used for histopathological examination. The protocol of the human study was reviewed and approved by the Tokyo Medical and Dental University Ethics Committee (No. 110). Written informed consent was obtained from all patients after they had been told that part of the resected brain specimen would be used not for diagnostic purposes, but purely for research. All procedures on animals were in accordance with the Tokyo Metropolitan Institutes of Gerontology Guide for the Care and Use of Laboratory Animals. Human cortical brain slices were transported to our PET facility, which is located far from the operating room in Tokyo Medical and Dental University. During transportation (40 min), brain slices were preincubated with Krebs–Ringer medium and bubbled with 95% O_2/5% CO_2 from a portable gas cylinder, and the temperature was maintained at 34 °C with a thermostat (Sasaki and Abe, 2001). Rat brain slices were preincubated in a chamber filled with the same medium and bubbled with 95% O_2/5% CO_2 for 45 min at 34 °C.

Bioradiographic study using FDG

FDG was synthesized by the method of Hamacher et al. (1986). The bioradiographic study was carried out using methods described previously (Sasaki et al., 2002a,b). There were two incubation conditions, control and high K^+. The chamber was filled with 100 ml of Krebs–Ringer medium (124 mM NaCl, 5 mM KCl, 2 mM $CaCl_2$, 1 mM $MgCl_2$, 1.2 mM KH_2PO_4, 26 mM $NaHCO_3$ and 10 mM glucose) as the control condition and that of high K^+ medium (79 mM NaCl, 50 mM KCl, 2 mM $CaCl_2$,

1 mM $MgCl_2$, 1.2 mM KH_2PO_4, 26 mM $NaHCO_3$ and 10 mM glucose) as the high K^+ condition, and placed them in the incubator at 34 °C. A continuous flow of 95% O_2/5% CO_2 gas was supplied to the medium. The brain slices were pre-incubated with Krebs–Ringer medium for the control incubation. A set of four human brain slices and of eight rat brain slices was transferred on a nylon net in the chamber and incubated with 37 MBq of FDG for 250 min. Two-dimensional images of radioactivity in the slices were recorded on a Storage Phosphor Screen through a thin polyvinylidene chloride sheet placed at the bottom of the chamber. Dynamic changes of radioactivity in the slices were measured by exposing the Storage Phosphor Screen for 10 min and changing it every 30 min. Autoradiographic images recorded on the Storage Phosphor Screen were read with a PhosphoImager SI and analyzed with IQMac v.1.2 to obtain images. ROIs were placed on regions of gray and white matter in images of the human neocortex and the rat cerebrum. Radioactivity was expressed as "counts/pixel/10 min", which represents radioactivity per unit area per 10 min of exposure. For the quantitative analysis, the values were decay-corrected to those at the start of incubation with FDG (37 MBq). Values on the ROIs were averaged and expressed as FDG uptake (mean±SD). In each experiment, the relation between FDG uptake and time of incubation was plotted from time 0 to 250 min as in Fig. 2 and the linear relation was expressed as a slope (counts/pixel/min). The slope of the gray matter in control and high K^+ media, and uptake ratio between high K^+/control media were compared with SG/CG and SG/CB uptake ratios obtained by PET. After the dynamic autoradiographic study, the brain slices in the chamber were observed with a microscope (SZX-12-3121, Olympus Optical Co. Ltd., Tokyo, Japan) equipped with a digital camera (Coolpix 100, Nikon Co., Ltd., Tokyo, Japan) and photographed for anatomical identification.

Statistical analysis

The bioradiographic uptake in gray matter was expressed as the rate of uptake per pixel per minute (counts/pixel/min) in control medium and that in high K^+ medium and the uptake ratio between high K^+/control media. The values were expressed as the mean±SD for 7 patients and 6 rats. The homoscedasticity in the uptake rate and the uptake ratio between rat and human tissues was analyzed with the F test. Statistical significance was determined using the Wilcoxon/Kruskal–Wallis test for differences of data with an outlier (arrow in Fig. 4) and without an outlier.

The magnitude of the relationship between FDG-PET and FDG bioradiographic data with an outlier (7 patients) and without an outlier (6 patients) was determined by a regression analysis. The statistical significance of the correlation was calculated using an F test.

Acknowledgment

REFERENCES

Ardekani, B.A., Braun, M., Hutton, B.F., Kanno, I., Iida, H., 1995. A fully automatic multimodality image registration algorithm. J. Comput. Assist. Tomogr. 19, 615–623.

Cascino, G.D., 2004. Surgical treatment for extratemporal epilepsy. Curr. Treat. Options Neurol. 6, 257–262.

Casse, R., Rowe, C.C., Newton, M., Berlangieri, S.U., Scott, A.M., 2002. Positron emission tomography and epilepsy. Mol. Imaging Biol. 4, 338–351.

Cohen-Gadol, A.A., Wilhelmi, B.G., Collignon, F., White, J.B., Britton, J.W., Cambier, D.M., Christianson, T.J., Marsh, W.R., Meyer, F.B., Cascino, G.D., 2006. Long-term outcome of epilepsy surgery among 399 patients with nonlesional seizure foci including mesial temporal lobe sclerosis. J. Neurosurg. 104, 513–524.

Cornford, E.M., Hyman, S., Swartz, B.E., 1994. The human brain GLUT1 glucose transporter: ultrastructural localization to the blood–brain barrier endothelia. J. Cereb. Blood Flow Metab. 14, 106–112.

Cornford, E.M., Hyman, S., Cornford, M.E., Landaw, E.M., Delgado-Escueta, A.V., 1998. Interictal seizure resections show two configurations of endothelial Glut1 glucose transporter in the human blood–brain barrier. J. Cereb. Blood Flow Metab. 18, 26–42.

Debets, R.M., Sadzot, B., van Isselt, J.W., Brekelmans, G.J., Meiners, L.C., van Huffelen, A.O., Franck, G., van Veelen, C.W., 1997. Is ^{11}C-flumazenil PET superior to ^{18}FDG PET and ^{123}I-iomazenil SPECT in presurgical evaluation of temporal lobe epilepsy? J. Neurol., Neurosurg. Psychiatry 62, 141–150.

During, M.J., Spencer, D.D., 1993. Extracellular hippocampal glutamate and spontaneous seizure in the conscious human brain. Lancet 341, 1607–1610.

Fazekas, F., Kapeller, P., Schmidt, R., Stollberger, R., Varosanec, S., Offenbacher, H., Fazekas, G., Lechner, H., 1995. Magnetic resonance imaging and spectroscopy findings after focal status epilepticus. Epilepsia 36, 946–949.

Graham, D.I., Lantos, P.L., 2002. Greenfield's Neuropathology, 7th ed. Arnold, London.

Hamacher, K., Coenen, H.H., Stocklin, G., 1986. Efficient stereospecific synthesis of no-carrier-added 2-[^{18}F]-fluoro-2-deoxy-D-glucose using aminopolyether supported nucleophilic substitution. J. Nucl. Med. 27, 235–238.

Honegger, P., Pardo, B., 1999. Separate neuronal and glial Na^+, K^+-ATPase isoforms regulate glucose utilization in response to membrane depolarization and elevated extracellular potassium. J. Cereb. Blood Flow Metab. 19, 1051–1059.

Huang, S.C., Phelps, M.E., Hoffman, E.J., Sideris, K., Selin, C.J., Kuhl, D.E., 1980. Noninvasive determination of local cerebral metabolic rate of glucose in man. Am. J. Physiol. 238, E69–E82.

Kumlien, E., Hartvig, P., Valind, S., Oye, I., Tedroff, J., Langstrom, B., 1999. NMDA-receptor activity visualized with (S)-[N-methyl-^{11}C]ketamine and positron emission tomography in patients with medial temporal lobe epilepsy. Epilepsia 40, 30–37.

Matheja, P., Weckesser, M., Debus, O., Lottgen, J., Schuierer, G., Schober, O., Kurlemann, G., 2000. Drug-induced changes in cerebral glucose consumption in bifrontal epilepsy. Epilepsia 41, 588–593.

Mtsumura, K., Bergstrom, M., Onoe, H., Takechi, H., Westerberg, G., Antoni, G., Bjurling, P., Jacobson, G.B., Langstrom, B., Watanabe, Y., 1995. In vitro positron emission tomography (PET): use of positron emission tracers in functional imaging in living brain slices. Neurosci. Res. 22, 219–229.

McGeer, P.L., Kamo, H., Harrop, R., McGeer, E.G., Martin, W.R., Pate, B.D., Li, D.K., 1986. Comparison of PET, MRI, and CT with pathology in a proven case of Alzheimer's disease. Neurology 36, 1569–1574.

Meldrum, B.S., 2000. Glutamate as a neurotransmitter in the brain: review of physiology and pathology. J. Nutr. 130 (4S Suppl.), 1007S–1015S.

Minoshima, S., Cross, D.J., Foster, N.L., Henry, T.R., Kuhl, D.E., 1999. Discordance between traditional pathologic and energy metabolic changes in very early Alzheimer's disease. Pathophysiological implications. Ann. N. Y. Acad. Sci. 893, 350–352.

Murata, T., Matsumura, K., Onoe, H., Bergstrom, M., Takechi, H., Sihver, S., Sihver, W., Neu, H., Andersson, Y., Ogren, M., Fasth, K.J., Langstrom, B., Watanabe, Y., 1996. Receptor imaging technique with ^{11}C-labeled receptor ligands in living brain slices: its application to time-resolved imaging and saturation analysis of benzodiazepine receptor using [^{11}C]Ro15-1788. Neurosci. Res. 25, 145–154.

Petroff, O.A., Errante, L.D., Rothman, D.L., Kim, J.H., Spencer, D.D., 2002. Glutamate–glutamine cycling in the epileptic human hippocampus. Epilepsia 43, 703–710.

Pfund, Z., Chugani, D.C., Juhasz, C., Muzik, O., Chugani, H.T., Wilds, I.B., Seraji-Bozorgzad, N., Moore, G.J., 2000. Evidence for coupling between glucose metabolism and glutamate cycling using FDG PET and 1H magnetic resonance spectroscopy in patients with epilepsy. J. Cereb. Blood Flow Metab. 20, 871–878.

Reivich, M., Alavi, A., Wolf, A., Fowler, J., Russell, J., Arnett, C., MacGregor, R.R., Shiue, C.Y., Atkins, H., Anand, A., Dann, R., Greenberg, J.H., 1985. Glucose metabolic rate kinetic model parameter determination in humans: the lumped constants and rate constants for [^{18}F]fluorodeoxyglucose and [^{11}C] deoxyglucose. J. Cereb. Blood Flow Metab. 5, 179–192.

Sasaki, T., Abe, K., 2001. Development of a transportable incubator for autoradiographic experiments with positron emitter-labeled tracers in living brain tissues. Brain Res. Brain Res. Protoc. 8, 170–175.

Sasaki, T., Ishiwata, K., Murata, T., Senda, M., 2002a. Demonstration of competition between endogenous dopamine and [^{11}C]raclopride binding in in vitro brain slices using a dynamic autoradiography technique. Synapse 44, 42–50.

Sasaki, T., Kawamura, K., Tanaka, Y., Ando, S., Senda, M., 2002b. Assessment of choline uptake for the synthesis and release of acetylcholine in brain slices by a dynamic autoradiographic technique using [^{11}C]choline. Brain Res. Brain Res. Protoc. 10, 1–11.

Sibson, N.R., Shen, J., Mason, G.F., Rothman, D.L., Behar, K.L., Shulman, R.G., 1998. Functional energy metabolism: in vivo ^{13}C-NMR spectroscopy evidence for coupling of cerebral glucose consumption and glutamatergic neuronal activity. Dev. Neurosci. 20, 321–330.

Sokoloff, L., 1999. Energetics of functional activation in neural tissues. Neurochem. Res. 24, 321–329.

Sokoloff, L., Takahashi, S., Gotoh, J., Driscoll, B.F., Law, M.J., 1996. Contribution of astroglia to functionally activated energy metabolism. Dev. Neurosci. 18, 344–352.

Somjen, G.G., 1975. Electrophysiology of neuroglia. Annu. Rev. Physiol. 37, 163–190.

Takahashi, S., Driscoll, B.F., Law, M.J., Sokoloff, L., 1995. Role of sodium and potassium ions in regulation of glucose metabolism in cultured astroglia. Proc. Natl. Acad. Sci. U. S. A. 92, 4616–4620.

Velisek, L., Moshe, S.L., 2003. Temporal lobe epileptogenesis and epilepsy in the developing brain: bridging the gap between the laboratory and the clinic. Epilepsia 44, 51–59.

Zheng, L., Godfrey, D.A., Waller, H.J., Godfrey, T.G., Chen, K., Sun, Y., 2000. Effects of high-potassium-induced depolarization on amino acid chemistry of the dorsal cochlear nucleus in rat brain slices. Neurochem. Res. 25, 823–835.

Neural correlates of regional EEG power change

N. Oishi,[a] T. Mima,[a,d,*] K. Ishii,[b,d] K.O. Bushara,[c,d] T. Hiraoka,[e] Y. Ueki,[a]
H. Fukuyama,[a] and M. Hallett[d]

[a]Human Brain Research Center, Kyoto University Graduate School of Medicine, Kyoto 606-8507, Japan
[b]Positron Medical Center, Tokyo Metropolitan Institute of Gerontology, 35-2 Sakaecho, Itabashi, Tokyo 173-0015, Japan
[c]Neurology service, Rm 4B135, Minneapolis Veterans Affairs Medical Center, One Veterans Drive, Minneapolis, MN 55417, USA
[d]NINDS, National Institutes of Health, Bethesda, MD 20892, USA
[e]Department of Radiology, Kyoto City hospital, Mibu-takadahigasi-cho, Nakagyo-ku, Kyoto 604-8845, Japan

To clarify the physiological significance of task-related change of the
regional electroencephalogram (EEG) rhythm, we quantitatively
evaluated the correlation between regional cerebral blood flow (rCBF)
and EEG power. Eight subjects underwent $H_2^{15}O$ positron emission
tomography scans simultaneously with EEG recording during the
following tasks: rest condition with eyes closed and open, self-paced
movements of the right and left thumb and right ankle. EEG signals
were recorded from the occipital and bilateral sensorimotor areas.
Cortical activation associated with EEG rhythm generation was
studied by the correlation between rCBF and EEG power. There were
significant negative correlations between the sensorimotor EEG
rhythm at 10–20 Hz on each side and the ipsilateral sensorimotor
rCBF and between the occipital EEG rhythm at 10–20 Hz and the
occipital rCBF. The occipital EEG rhythm showed a positive
correlation with the bilateral medial prefrontal rCBF, while the right
sensorimotor EEG rhythm showed a positive correlation with the left
prefrontal rCBF. In conclusion, decrease in the regional EEG rhythm
at 10–20 Hz might represent the neuronal activation of the cortex
underlying the electrodes, at least for the visual and sensorimotor
areas. The neural network including the prefrontal cortex could play
an important role to generate the EEG rhythm.
© 2007 Elsevier Inc. All rights reserved.

Keywords: Neural networks; Positron emission tomography (PET);
Regional cerebral blood flow; Sensorimotor; Visual

Introduction

The electroencephalogram (EEG) represents the summed
postsynaptic potentials of cortical neurons (Niedermeyer and
Lopes da Silva, 1987). The generator mechanisms of EEG rhythm
in various frequency bands, however, are not well understood.

In normal subjects, the EEG rhythm at 8–12 Hz is usually most
conspicuous over the parieto-occipital area (Berger, 1929;
Pfurtscheller and Lopes da Silva, 1999) and is called the occipital
alpha band rhythm. The EEG alpha band rhythm may be associated
with the alert and yet relaxed state and is commonly used as an
indirect measure of the functional organization of brain. It is well
known that normal awake alpha band rhythms are 'blocked'
(substantially reduced in amplitude) by eye opening and moderate
to difficult mental tasks (Berger, 1930, 1932; Nunez et al., 2001;
Vijn et al., 1991). Thus, some authors suggested that the occipital
alpha band rhythm might be considered as an idling rhythm of
visual areas (Kuhlman, 1978).

One of the most relevant activities overlapping the occipital
alpha band rhythm is the so-called mu rhythm which is restricted
over the hand area of the primary sensorimotor cortex (SM1) and
is suppressed not by eye opening but by active hand movements.
The sensorimotor mu rhythm could also be considered as an
idling rhythm of sensorimotor areas (Kuhlman, 1978; Pfurtscheller,
1992). Although the role of the thalamocortical circuitry in the
generation of sleep spindles has been emphasized (Steriade et al.,
1990), the neurophysiological mechanisms by which the regional
alpha band rhythm such as the occipital alpha or the sen-
sorimotor mu rhythm are to be generated or suppressed are still
unclear.

Higher frequency EEG waves such as the beta band rhythm
(13–30 Hz) are associated with the cortical activation most
pronounced during the awake state and rapid eye movement sleep
(Nofzinger et al., 2000). During various motor tasks, EEG studies
showed a transient decrease of EEG power in the beta band
(Pfurtscheller, 1989), which is called event-related desynchroniza-
tion (ERD) (Pfurtscheller, 1977; Pfurtscheller and Aranibar, 1977)

or task-related power decrease (Gerloff et al., 1998). This decrease starts 1–2 s prior to the movement onset and is followed by a rebound-like increase just after termination of the movement (event-related synchronization: ERS) (Pfurtscheller, 1992). It is speculated that the motor cortex shifts from an activated state during preparation and execution of movement (working cortex) to a resting state after termination of movement or, in other words, from a processing mode to an 'idling' mode (Pfurtscheller et al., 1996). This hypothesis is also supported by a transcranial magnetic stimulation study showing decreased corticospinal excitability at the time of the 20-Hz event-related synchronization (Chen et al., 1998). However, the generator mechanism of regional beta band rhythm is still unknown.

Brain electrical activity represents the single greatest demand on cerebral metabolism (Erecinska and Silver, 1989), suggesting that measurement of electrical energy also should be coupled to cerebral metabolism and perfusion. In normal subjects, cerebral glucose uptake and blood flow are generally accepted as tightly coupled measures of cerebral energy utilization (Sokoloff, 1977, 1981). The association between EEG power and cerebral glucose metabolism has been occasionally studied using the 18-fluoro-deoxyglucose positron emission tomography (PET) technique (Larson et al., 1998; Oakes et al., 2004; Schreckenberger et al., 2004). However, a limitation of the 18-fluoro-deoxyglucose tracer is that over the span of 30 min it is difficult to ensure that the subject remains in the same functional state (Oakes et al., 2004). Regional cerebral blood flow (rCBF) has been used as an indirect measure of functional neural activity (Raichle, 1987) and the PET technique is considered to be the 'gold standard' in CBF measurements in humans (Feng et al., 2004). Measurement of rCBF using $H_2{}^{15}O$ PET has been well established based on the single-tissue compartment model for diffusible tracers in at least physiologically normal brain tissue (Sadato et al., 1998). The $H_2{}^{15}O$ tracer has shorter time frame (10–30 s) than the 18-fluoro-deoxyglucose tracer (20–30 min) and the results of $H_2{}^{15}O$ PET examinations directly depend on the acute cerebral state of activation during tracer injection (Schreckenberger et al., 2004). In normal subjects, cerebral blood flow is generally accepted as tightly coupled measures of cerebral energy utilization (Sokoloff, 1977, 1981). It was reported that EEG power showed strong associations with rCBF in most frequency bands including the alpha and beta range (Leuchter et al., 1999). Therefore, taken together with the EEG power change described above, it is predicted that rCBF associated with the neuronal activation might covary with the EEG power in at least normal subjects. Although previous reports (Ingvar et al., 1976; Paulson and Sharbrough, 1974) mentioned the relationship between EEG and rCBF in humans, the record of EEG and rCBF could not be done simultaneously due to limitations in the EEG and rCBF technique. Recently, the association between EEG power and rCBF recorded simultaneously has been occasionally studied using the $H_2{}^{15}O$ technique (Leuchter et al., 1999; Nakamura et al., 1999; Sadato et al., 1998). However, the previous reports investigated a correlation between rCBF and the EEG rhythm averaged across the whole scalp. The averaged EEG rhythm might be inappropriate to investigate regional EEG power change such as sensorimotor mu rhythm because the occipital alpha band rhythm may diminish an effect of sensorimotor mu rhythm in the averaged alpha power. Therefore, it would be preferable to investigate the relationship between rCBF change induced by several tasks and the regional EEG rhythm to clarify

neurophysiological mechanisms in the generation or suppression of the regional EEG power. To achieve this goal, we employed rather simple tasks that are commonly used in clinical EEG recording.

The purpose of the present study is to quantitatively evaluate the correlation between rCBF changes using $H_2{}^{15}O$ PET and EEG power changes induced by several motor tasks and clarify what brain regions are involved in the generation and suppression of the regional EEG rhythms.

Methods

Subjects

Eight right-handed healthy volunteers (5 males and 3 females; mean age±SD, 42±10 years) participated in the experiment. The protocol was approved by the NINDS Institutional Review Board and the NIH Radiation Safety Committee. All subjects gave their written informed consent for the study and had no medical history of neurological or psychiatric disorders.

Tasks

The subjects lay in a supine position and the following tasks were performed twice for each (total 10 times):

1. rest condition with eyes closed (EC)
2. rest condition with eyes open (EO)
3. self-paced right thumb abduction and adduction movement (1–2 Hz) with eyes closed (RH)
4. self-paced left thumb abduction and adduction movement (1–2 Hz) with eyes closed (LH)
5. self-paced right ankle extension and flexion movement (1–2 Hz) with eyes closed (RF)

The order of tasks was randomized across subjects. Electrophysiological recording and PET scanning were carried out simultaneously in all conditions (Fig. 1).

Electrophysiological recording

EEG signals were recorded from 6 electrodes (O1, O2, C3, C4, FC3, FC4 according to the International 10–20 System) secured with collodion and referenced to the right earlobe electrode (A2). The left earlobe electrode (A1) was recorded as a separate channel. To reliably estimate the scalp EEG potential, we converted the EEG signals into the digitally linked earlobe reference before further analysis (Mima and Hallett, 1999; Nunez et al., 1997). A previous study showed that the electrode locations of FC3/C3, FC4/C4 and O1/O2 are just over the left and right SM1 and the occipital cortex, respectively (Steinmetz et al., 1989). Electromyogram (EMG) signals were recorded from 5 muscles (right abductor pollicis brevis [APB], biceps [BIC], left APB, BIC and right hamstring). To monitor the eye movement and blinking, electro-oculograms (EOGs) were monitored by pairs of electrodes placed at the left and right lateral canthus for horizontal eye movement and by another pair of electrodes placed below and above the right eye for vertical eye movement. To monitor tongue movement, a surface electrode placed at the upper edge of the right nasolabial fold
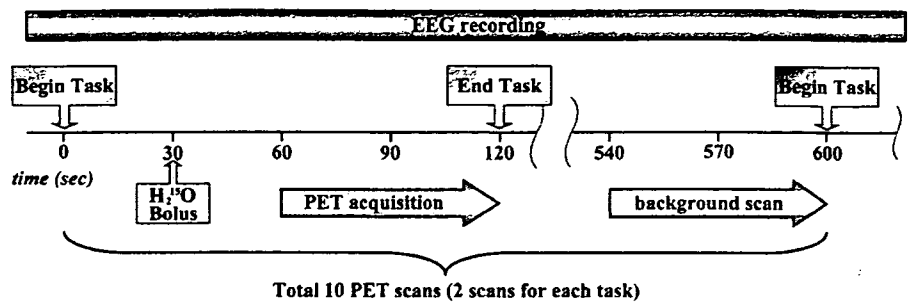
Fig. 1. Sequence and time course of the EEG/PET/task protocol.

and referenced to linked earlobe electrodes was used to record the glossokinetic potential. Impedance was kept below 5 kΩ. EEG and EMG signals were amplified and filtered by bandpass of 1–50 Hz and 10–50 Hz, respectively, and both were digitized at 250 Hz (Neuroscan, Neuroscan Inc. Herndon, VA). EEG and EMG signals during both conditions were segmented into non-overlapping and artifact-free epochs of 1024 ms which allowed a 1-Hz frequency resolution after Fourier transformation. Epochs with unwanted muscle activity were excluded from the analysis. Power spectra were computed by a fast Fourier transform algorithm implemented on the Neuroscan software. Based on the previous studies (Andres et al., 1999; Mima et al., 2000), the power spectra were grouped into four different frequency bands, 8–12 Hz (alpha), 13–20 Hz (beta1), 21–30 Hz (beta2), and 31–50 Hz (gamma). Since the high and low alpha band rhythms (Klimesch, 1999) behaved quite similarly in our experiment using the simple tasks, we analyzed the whole alpha band as one group. Although the gamma band activity is of special importance for cognition (Rodriguez et al., 1999; Tallon-Baudry and Bertrand, 1999), we did not analyze the gamma band activity because of the environmental electromagnetic noise in the PET scanning room and the possible contamination of EMG. In addition to the 60 Hz noise, the possible contamination of the muscle activity to the occipital electrodes because of the increased neck muscle tone was inevitable due to the tight head fixation for the PET scanning in a few subjects. The local EEG power was calculated by the averaging the EEG powers at 2 electrodes (FC3/C3, FC4/C4, and O1/O2) that were obtained during the PET procedure (60 s). A logarithmic transformation was applied to normalize the power (Halliday et al., 1995).

PET acquisition

$H_2^{15}O$ PET scans were obtained in 3D mode using a GE Advance PET tomograph (GE Medical System, Milwaukee, WI) with an axial field of view of 15.3 cm. The task performance began 30 s before bolus infusion of 10 mCi of $H_2^{15}O$ (half life 2.1 min) via a catheter in the left cubital vein. Scanning was started when a rising brain radioactivity count was first detected (20–30 s) after injecting the radio-isotope. Scanning continued for 60 s thereafter. Inter-scan interval was 10 min. A transmission scan obtained prior to each session was used to correct for attenuation. Head movement was minimized by using a thermoplastic mask that was molded to each subject's head and attached to the scanner bed. Each subject underwent 10

consecutive PET scans (2 scans for each task). The sequence and time course of the PET/EEG/task protocol are shown in Fig. 1.

Data analysis

The attenuation-corrected emission scans were reconstructed into 35 trans-axial planes, 4.25 mm apart, with an in-plane center resolution of 6.5 mm full width at half-maximum (FWHM) in each direction. Scans from each subject were realigned to correct the head motion during the study then normalized to a standard bicommissural stereotactic space (using Montreal Neurological Institute template) and smoothed with an isotropic Gaussian filter of 12 mm using SPM2 (Wellcome Department of Cognitive Neurology, London, UK) implemented in Matlab (Friston et al., 1990, 1991, 1995). After correction for variations in global blood flow (normalized to 50 ml/100 g/min) using analysis of covariance (ANCOVA), the multi-subject, covariate only design matrix was specified and the subjects with logarithmic EEG power during each task as a covariate were estimated according to the general linear model at each and every voxel, assuming a linear relationship between rCBF and the covariate. Both positive and negative correlations at each voxel were estimated for the occipital, left sensorimotor, and right sensorimotor EEG power. Therefore, the EEG bands of alpha, beta1, and beta2 were adopted in the right and left sensorimotor and occipital regions and a total of 9 covariates were included in separate design matrices. The occipital EEG power was also considered in both sensorimotor EEG power analyses as a nuisance factor because the occipital alpha and beta EEG could have an influence on the sensorimotor EEG.

The resulting whole brain statistical parametric maps of *t*-statistic (SPM(*t*)) had a final spatial resolution of 12.6×13.7× 15.0 mm FWHM. The SPM(*t*) map was transformed into units of normal distribution (SPM(z)), where the significance of each region was estimated with a threshold of uncorrected $p < 0.001$. This uncorrected threshold is commonly used in SPM (Benoit et al., 2002; Salmon et al., 2000; Staff et al., 2000). Because of a large number of statistical comparisons in this voxel-by-voxel analysis, the Bonferroni correction was done to eliminate the probability of a type-I error. Because the Bonferroni correction is the most conservative correction for multiple comparisons and might result in a type-II error, statistical parametric maps that survived a threshold of $p < 0.001$ uncorrected for multiple comparisons were also shown. A higher threshold presented by a corrected $p < 0.05$ at cluster levels was also applied in order to

exclude the clusters that have any probability of being randomly produced (Bench et al., 1992; Salmon et al., 2000; Staff et al., 2000). The SPM coordinates for standard brain from Montreal Neurological Institute were converted to Talairach coordinates (Talairach and Tournoux, 1988) by a non-linear transform method (see http://www.mrc-cbu.cam.ac.uk/Imaging/Common/mnispace. shtml).

Results

The mean movement frequencies during the tasks (task 3, 4 and 5) were 1.3±0.3 Hz in RH, 1.2±0.2 Hz in LH and 1.3± 0.3 Hz in RF (no significant differences). The mean EEG alpha frequencies were 9.8±0.9 Hz in the occipital area, 10.8± 2.1 Hz in the left sensorimotor area and 11.0±1.5 Hz in the right sensorimotor area (no significant differences). The logarithmic regional EEG band power is shown in Fig. 2.

Brain regions correlated with the occipital EEG power

A significant negative correlation between the occipital alpha power and rCBF was found in the bilateral occipital cortices including the primary and association visual cortex (Fig. 3A, Table 1A). Similarly a negative correlation between the occipital beta1 power and rCBF was found in the bilateral occipital cortices (Fig. 3B, Table 1A). A significant negative correlation between the occipital beta2 power and rCBF was found in the posterior part of the right middle temporal gyrus (Fig. 3C, Table 1A). A significant positive correlation between the occipital alpha power and rCBF was found in both lateral and medial prefrontal cortices and basal forebrain mainly on the left. The left superior temporal gyrus also showed a positive correlation (Fig. 3A, Table 1B). A significant positive correlation between the occipital beta1 power and rCBF was also found in both lateral and medial prefrontal cortices and the left superior temporal gyrus (Fig. 3B, Table 1B). No significant positive correlation was found between the occipital beta2 power and rCBF was found (Fig. 3C, Table 1B).

Brain regions correlated with the left sensorimotor EEG power

A significant negative correlation between the left sensorimotor alpha power and rCBF was found in the left pre- and postcentral gyrus and the left inferior parietal lobule (Fig. 4A, Table 2A). A significant negative correlation between the left sensorimotor beta1 power and rCBF was also found in the left pre- and postcentral gyrus (Fig. 4B, Table 2A). A significant negative correlation between the left sensorimotor beta2 power and rCBF was found in the left postcentral gyrus and inferior parietal lobule (Fig. 4C, Table 2A). No significant positive correlation between the left sensorimotor EEG power and rCBF was found (Figs. 4A–C, Table 2B).
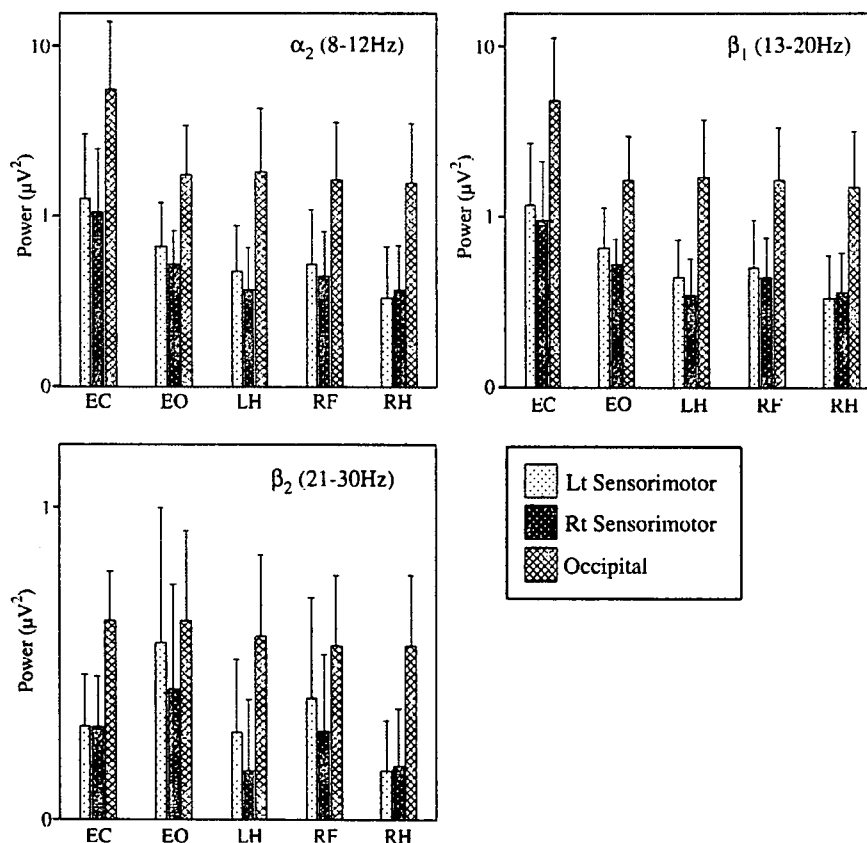

Fig. 2. Plot (mean values+standard deviation) of absolute regional EEG band power. EC, eyes closed; EO, eyes open; LH, left thumb movement; RH, right thumb movement; RF, right foot movement.
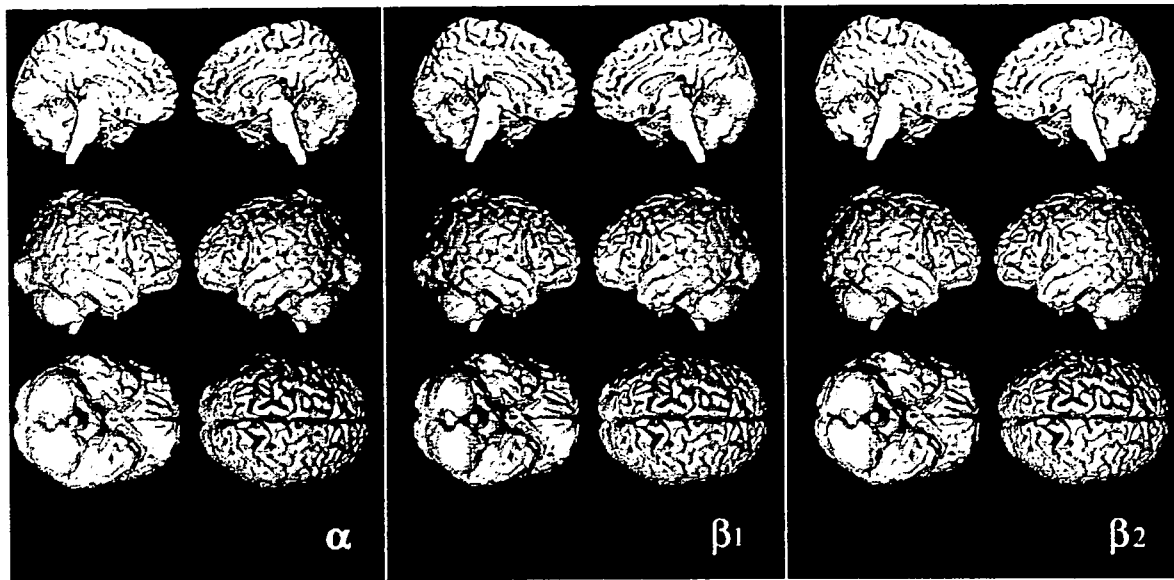
Fig. 3. Statistical parametric maps of positive (yellow-red) and negative (aqua-blue) correlation between rCBF and occipital EEG alpha, beta1 and beta2 power during each task, superimposed on surface-rendered MRI. Areas that survived a statistical threshold of $p < 0.001$ uncorrected for multiple comparisons are shown. A significant negative correlation between the occipital alpha and beta1 power and rCBF was found in the bilateral occipital cortices. A significant positive correlation between the occipital alpha and beta1 power and rCBF was also found in both lateral and medial prefrontal cortices.

Brain regions correlated with the right sensorimotor EEG power

A significant negative correlation between the right sensorimotor alpha power and rCBF was found in the right postcentral gyrus and inferior parietal lobule (Fig. 5A, Table 3A). A significant negative correlation between each of the right sensorimotor beta1 and beta2 power and rCBF was also found in the right postcentral gyrus and inferior parietal lobule (Figs. 5B–C, Table 3A). A significant positive correlation between the right sensorimotor alpha power and rCBF was found in the left middle frontal gyrus (Fig. 5A, Table 3B).

Table 1
Brain regions (A) negatively and (B) positively correlated with the occipital EEG power

EEG band	Region	BA	Coordinate Talairach space			Cluster-level corrected P	kE	z
			x	y	z			
(A) Negative correlation								
Alpha	Rt lingual gyrus (GL)	19	20	−78	−11	0.000	9807	5.49
	Rt cuneus	18	10	−101	9			5.35
	Lt lingual gyrus (GL)	18	−8	−80	−13			5.29
	Lt fusiform gyrus (GF)	19	−22	−53	−11	0.003	456	5.10
Beta1	Rt lingual gyrus (GL)	19	20	−11	−11	0.000	9278	5.33
	Lt lingual gyrus (GL)	18	−8	−80	−13			5.16
	Rt cuneus	18	10	−101	9			5.12
	Lt fusiform gyrus (GF)	19	−24	−53	−12	0.006	398	4.99
Beta2	Rt middle temporal gyrus (GTm)	37	50	−62	3	0.011	358	4.10
(B) Positive correlation								
Alpha	Lt anterior cingulate	32	−8	44	−9	0.000	6018	5.27
	Lt superior temporal gyrus (GTs)	38	−49	22	−18	0.000	882	4.60
	Lt precentral gyrus (GPrC)	9	−38	13	34	0.025	289	4.34
	Lt middle frontal gyrus (GFm)	8	−46	10	42			3.62
	Rt middle frontal gyrus (GFm)	8	30	31	43	0.006	399	4.23
Beta1	Rt anterior cingulate	32	12	29	−6	0.000	5714	5.30
	Lt anterior cingulate	32	−8	44	−7			5.16
	Lt superior temporal gyrus (GTs)	38	−49	22	−18	0.000	703	4.39
	Rt middle frontal gyrus (GFm)	8	32	31	41	0.002	507	4.20
	Rt superior frontal gyrus (GFs)	8	40	20	51			3.65
Beta2	No suprathrethold clusters							

Clusters that survived a statistical threshold of $p < 0.05$ corrected for multiple comparisons are shown.
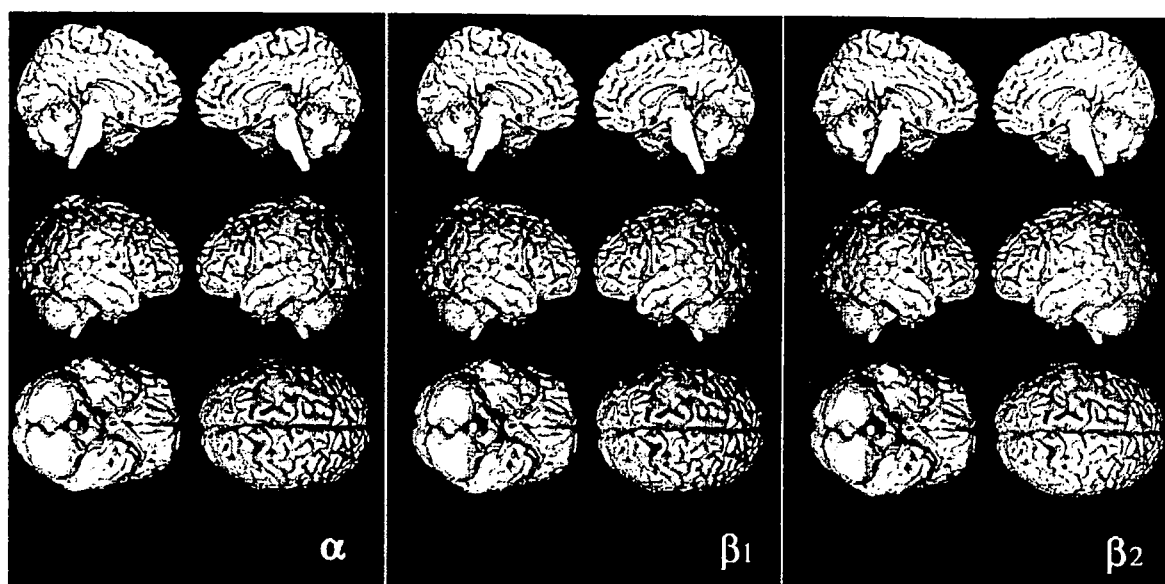
Fig. 4. Statistical parametric maps of positive (yellow-red) and negative (aqua-blue) correlation between rCBF and left sensorimotor EEG alpha, beta1 and beta2 power during each task, superimposed on surface-rendered MRI. Areas that survived a statistical threshold of $p < 0.001$ uncorrected for multiple comparisons are shown. A significant negative correlation between the left sensorimotor alpha and beta1 power and rCBF was found in the left pre- and postcentral gyrus. A significant negative correlation between the left sensorimotor beta2 power and rCBF was found in the left postcentral gyrus.

A significant positive correlation between the right sensorimotor beta1 power and rCBF was found in the left lateral prefrontal cortex and the left superior occipital gyrus (Fig. 5B, Table 3B). No significant positive correlation was found between the right sensorimotor beta2 power and rCBF was found (Fig. 5C, Table 3B).

Discussion

This is the first report of quantitative evaluation of the correlation between rCBF changes and regional EEG powers. Significant negative correlations between the occipital EEG power within the

alpha and lower beta bands and the occipital rCBF were observed. There were also significant negative correlations between the left and right sensorimotor EEG power within the alpha and beta ranges and the ipsilateral sensorimotor rCBF, respectively. These findings suggest that decrease in the regional EEG rhythm at around 10–20 Hz might represent the neuronal activation of the cortex underlying the electrodes, at least for the visual and sensorimotor areas. Since the animal experiments suggested that low amplitude desynchronized EEG is associated with the increased excitability in thalamocortical system (Steriade and Llinas, 1988), it is possible that the decrease of human scalp-recorded EEG power reflects cortical activation (Pfurtscheller, 1992).

Table 2
Brain regions (A) negatively and (B) positively correlated with the left sensorimotor EEG power

EEG band	Region	BA	Coordinate Talairach space			Cluster-level corrected P	kE	z
			x	y	z			
(A) Negative correlation								
Alpha	Lt precentral gyrus (GPrC)	4	−32	−25	51	0.000	1550	5.19
	Lt postcentral gyrus (GPoC)	3	−38	−19	47			5.06
	Lt inferior parietal lobule (LPi)	40	−40	−31	35			3.70
Beta1	Lt precentral gyrus (GPrC)	4	−30	−25	49	0.000	1396	4.96
	Lt postcentral gyrus (GPoC)	3	−38	−19	47			4.79
Beta2	Lt postcentral gyrus (GPoC)	2	−51	−21	45	0.000	964	4.58
	Lt inferior parietal lobule (LPi)	40	−42	−27	42			3.95
	Lt postcentral gyrus (GPoC)	40	−61	−22	18			3.52
(B) Positive correlation								
Alpha	No suprathrethold clusters							
Beta1	No suprathrethold clusters							
Beta2	No suprathrethold clusters							

Clusters that survived a statistical threshold of $p < 0.05$ corrected for multiple comparisons are shown.
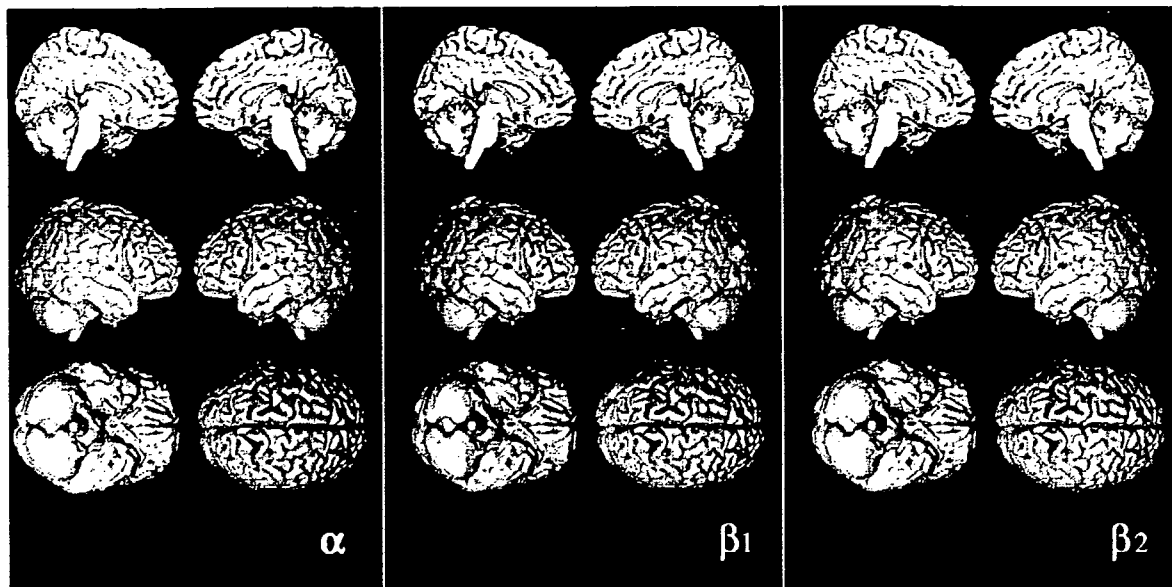
Fig. 5. Statistical parametric maps of positive (yellow-red) and negative (aqua-blue) correlation between rCBF and right sensorimotor EEG alpha, beta1 and beta2 power during each task, superimposed on surface-rendered MRI. Areas that survived a statistical threshold of $p < 0.001$ uncorrected for multiple comparisons are shown. A significant negative correlation between the right sensorimotor alpha, beta1 and beta2 power and rCBF was found in the right postcentral gyrus. A significant positive correlation between the right sensorimotor alpha and beta1 power and rCBF was found in the left middle frontal gyrus.

The occipital EEG power showed a positive correlation especially with the rCBF of the prefrontal cortex and the right sensorimotor EEG power showed a positive correlation with the rCBF of the left prefrontal cortex. These results suggest that the neural network including the prefrontal cortex especially on the left could play an important role to generate the EEG rhythm in both occipital and sensorimotor cortices.

Negative correlations of rCBF with the sensorimotor mu rhythm

By investigating the linear relationship between the sensorimotor alpha power and rCBF, we showed that the left and right mu rhythms have a significant negative correlation with the ipsilateral sensorimotor cortical activation. Because differences in source localization, frequency, power, and functional responsiveness suggest independent sources for mu and occipital alpha rhythms (Pineda, 2005), we performed the rCBF correlation analysis using SPM by setting the occipital alpha power as a statistical nuisance value to evaluate the purely sensorimotor mu rhythm, although the general linear model might not properly eliminate the "nuisance" effect. In addition, we evaluated multiple motor tasks in the present study to minimize a task-specific effect on rCBF change.

Although overlapping each other in the frequency range, the sensorimotor mu and occipital alpha band rhythms rather reflect

Table 3

Brain regions (A) negatively and (B) positively correlated with the right sensorimotor EEG power

EEG band	Region	BA	Coordinate Talairach space			Cluster-level corrected P	kE	z
			x	y	z			
(A) Negative correlation								
Alpha	Rt inferior parietal lobule (LPi)	40	40	−33	44	0.034	266	4.23
	Rt postcentral gyrus (GPoC)	3	36	−23	47			3.37
Beta1	Rt inferior parietal lobule (LPi)	40	42	−35	44	0.001	529	4.44
	Rt postcentral gyrus (GPoC)	3	36	−23	47			3.72
Beta2	Rt inferior parietal lobule (LPi)	40	46	−34	57	0.001	570	4.33
	Rt postcentral gyrus (GPoC)	40	44	−27	47			3.85
	Rt postcentral gyrus (GPoC)	3	53	−23	38			3.56
(B) Positive correlation								
Alpha	Lt middle frontal gyrus (GFm)	10	−32	49	−1	0.037	261	4.48
Beta1	Lt middle frontal gyrus (GFm)	10	−30	47	−2	0.048	242	4.28
	Lt inferior frontal gyrus (GFi)	10	−36	45	5			3.76
	Lt middle frontal gyrus (GFm)	11	−24	40	−9			3.33
	Lt superior occipital gyrus (GOs)	19	−32	−76	24	0.021	300	4.27
Beta2	No suprathreshold clusters							

Clusters that survived a statistical threshold of $p < 0.05$ corrected for multiple comparisons are shown.

two distinct physiological phenomena, which was also supported by the present results (Vanni et al., 1999). It has been reported that self-paced hand movement can induce a contralateral localized mu rhythm ERD and an occipital localized alpha band rhythm ERS at the same time (Pfurtscheller and Lopes da Silva, 1999). In direct recordings from cat visual and somatosensory cortices while both alpha and mu rhythms occurred under similar behavioral conditions, their bursts were independent and had low coherence (Rougeul-Buser and Buser, 1997).

In human scalp EEG, the main peak frequency of the mu rhythm is within the alpha band, which mainly covers a frequency range between 7 and 14 Hz with a mean frequency around 10 Hz or even slightly below (Pfurtscheller et al., 2000). However, its distribution is over the bilateral hand SM1, and its power is particularly sensitive to the motor tasks. The blocking of mu rhythm caused by movements of the body part is specific to somatic representation areas of the cortex (Arroyo et al., 1993). The time course of the mu rhythm amplitude shows a specific biphasic pattern, which is known as ERS/ERD (Pfurtscheller, 1977; Pfurtscheller and Lopes da Silva, 1999). Consequently, the 10-Hz mu rhythm increase might reflect a resting state or even inhibition in the sensorimotor system (Pfurtscheller, 1992; Salmelin and Hari, 1994). Our findings are in accord with the 'idling' rhythm hypothesis of the mu rhythm (Kuhlman, 1978). Moreover, the power suppression of the mu rhythm produced by a motor task (Crone et al., 1998; Gerloff et al., 1998; Pfurtscheller and Berghold, 1989; Toma et al., 2002; Toro et al., 1994) may reflect cortical activation at SM1 in a parametric way.

Although the limited spatial resolution of the rCBF measurement using PET cannot allow us to precisely differentiate S1 and M1, the parietal cortex including the postcentral gyrus and inferior parietal lobule showed a greater negative correlation than the frontal cortex including the precentral gyrus in this study. The previous PET study using a simple repetitive finger movement task also showed activation of both S1 and M1 (Mima et al., 1999). The activation of S1 may be due to the somatosensory afferent feedback from the periphery or the motor efferent copy conveyed from M1. It is also possible that the activity of S1 is related to preparation for motor action because some studies showed attenuation of the postcentral mu rhythm prior to voluntary movements (Nagamine et al., 1996; Ohara et al., 2000; Salmelin et al., 1995). Based on the recent results showing a specific motor deficit in movement initiation after an inferior parietal lobule lesion (Mattingley et al., 1998), the inferior parietal lobule has been suggested as a candidate area for higher-order motor function. Since coherent cell assemblies over at least several square centimeters are necessary (Cooper et al., 1965; Lopes da Silva, 1991) for the generation of the scalp-recorded EEG rhythmicity, both M1 and the parietal cortex are likely to be associated with the 'idling' of the mu rhythm.

Negative correlations of rCBF with the sensorimotor beta band rhythm

In this study, the activated areas that were negatively correlated with the sensorimotor alpha, beta1 and beta2 power showed similar cortical distributions. It has been well accepted that the beta band rhythm at SM1 might play an important role in motor control. Cortico-muscular coherence studies suggested that the central beta band rhythm may convey the motor command from M1 to the motor units (Conway et al., 1995; Mima et al., 2000; Salenius et

al., 1996). It has also been reported that the somatosensory beta band rhythms around 18 Hz in monkeys distribute over the SI hand area and the posterior parietal cortex and are blocked by the smallest body movement (Rougeul et al., 1979). Beta desynchronization during voluntary hand movement occurred in parallel with the mu ERD in the alpha band (Pfurtscheller, 1981).

Electrocorticogram and magnetoencephalography studies suggested that the 10 Hz rhythm could appear to arise from the somatosensory cortex, whereas the 20 Hz rhythm could arise predominantly from the precentral gyrus (Hari and Salmelin, 1997; Pfurtscheller, 1992; Salmelin et al., 1995; Salmelin and Hari, 1994). However, this topographic distribution is still controversial because electrocorticogram studies showed no consistent difference in distribution between the 10 Hz rhythm and the 20 Hz rhythm (Crone et al., 1998; Ohara et al., 2000). The rCBF changes in our study did not reveal this anterior–posterior tendency. However, this might be due to the limited spatial resolution of the PET methodology.

Negative correlations of rCBF with the occipital rhythm

The thalamocortical and corticocortical systems are supposed to interact in the generation of cortical alpha band rhythms (Steriade et al., 1990). In this study, the occipital alpha EEG had a significant negative correlation with the bilateral occipital rCBF, which extended broadly from the primary to association cortex. The result is in accordance with the previous reports (Leuchter et al., 1999; Sadato et al., 1998). Extensive involvement of the primary and association visual cortex is consistent with the finding that the alpha band rhythm can be suppressed not only by opening of the eyes but also by visual imagery, which suggests that the suppression of alpha band rhythm can be associated with higher visual processing (Hari and Salmelin, 1997).

Although previous studies revealed that the rCBF change (Larson et al., 1998; Sadato et al., 1998) or the glucose metabolic change (Schreckenberger et al., 2004) in the thalamus correlates with the global alpha power, our result showed no significant correlation between the regional occipital alpha EEG and the activation of thalamus. Therefore, it is possible that the generator mechanism of the whole brain alpha band rhythm and regional (occipital) alpha band rhythm might be different and that the thalamus is related to the production of the former but not so much for the latter. Electrophysiological evidence from isolated cerebral cortex determined that cortical circuits were capable of generating alpha band rhythms quite independently of thalamic influences (Kristiansen and Courtois, 1949). In addition, it has been reported that the corticocortical alpha coherence values were higher than any thalamocortical coherence (da Silva et al., 1973; Lopes da Silva et al., 1980) and relatively independent of thalamic influences (Lopes da Silva et al., 1980).

In this study, a similar correlation with rCBF was observed for the occipital alpha and beta1 power. When a subject concentrates on a particular modality, the EEG activity in the alpha and/or lower beta band specifically decreases in the corresponding brain region (Neuper and Pfurtscheller, 2001). Therefore, our result suggests that the same neurophysiological mechanism as the occipital alpha band rhythm could be associated with the occipital beta1 band rhythm generation. However, the similar correlation might be caused by a harmonic of the alpha activity because alpha activity is often not sinusoidal and it is very difficult to differentiate such a harmonic from beta band rhythms.

Positive correlations of rCBF with the sensorimotor and occipital rhythm

A significant positive correlation was found between the right sensorimotor alpha power and the rCBF of the left middle prefrontal gyrus, which extended to the dorsolateral prefrontal cortex (BA 9/46) (Ramnani and Owen, 2004). The sensorimotor mu rhythm is associated with motor behavior (Pfurtscheller et al., 1996). Although no direct connections have been reported between the dorsolateral prefrontal cortex and SM1, the dorsolateral prefrontal cortex sends the strongest projections to the premotor system in the macaque monkey brain (Lu et al., 1994). The premotor area could influence motor control (Tokuno and Nambu, 2000) via its dense corticocortical projections to M1 (Dum and Strick, 2002; Shimazu et al., 2004). Our result suggests that the corticocortical network between the prefrontal cortex and the SM1 via the premotor cortex might be associated with the generation of the sensorimotor mu rhythm, especially on the right. On the other hand, the left sensorimotor EEG power did not show any significant positive correlations. The EEG study using an independent component analysis suggested independent mu sources in the two hemispheres (Makeig et al., 2002). Therefore, the asymmetric results in our study might explain the independent generation of the sensorimotor mu rhythm in the two hemispheres. However, further researches would be necessary to elucidate the exact role of left middle frontal gyrus for the generation of mu rhythm.

A significant positive correlation between the right sensorimotor beta1 power and rCBF was found in the left lateral prefrontal cortex which is similar to the right sensorimotor mu power. Our result suggests that the corticocortical network including the prefrontal cortex and SM1 could be associated with the generation of the sensorimotor beta1 band rhythm as well as the mu rhythm in the alpha band. In a previous study (Nakamura et al., 1999), the rCBF in the left lateral prefrontal cortex was demonstrated to be positively correlated with the global beta power. Beta activity has recently been ascribed to the general role of an 'attention-carrier' (Wrobel, 2000) and associated with behavioral arousal and attentional processes (Nofzinger et al., 2000). States of attention and motor preparation were suggested to be particularly associated with increased levels of beta activity in the cat (Bouyer et al., 1981) and the monkey motor cortex (Rougeul et al., 1979) in local field potential studies. These reports suggest that focused attention for the motor preparation might be associated with the sensorimotor beta1 band rhythm and the prefrontal cortex (Steriade, 1993).

A significant positive correlation between the occipital alpha power and rCBF was found in both lateral and medial prefrontal cortices and basal forebrain mainly on the left, which is consistent with the previous study (Sadato et al., 1998) that showed a positive correlation between the alpha power and the rCBF in the limbic system including basal prefrontal cortex. A similar positive correlation was also found between the occipital beta1 power and rCBF. The orbitofrontal cortices are associated with social–affective and motivational aspects of frontal lobe function (Rolls, 2004). Anatomically, the orbitofrontal cortices have widespread connections with a distributed ascending activating system including the pontine reticular formation, basal forebrain, amygdala, hippocampus, temporal pole, insula, cingulate cortex and parahippocampal gyrus (Morecraft et al., 1992), placing them in a position to integrate limbic–paralimbic afferents with those coming from higher order association cortex and subsequently influence motivational, emotional and arousal systems in the brain (Nofzinger et al., 2000). The

positive correlation between the occipital alpha and beta1 power and neuronal activities in the limbic system including anterior cingulate cortex and orbitofrontal cortex may provide a neuroanatomical basis for studies of the relationship between emotional state and occipital alpha and beta1 band rhythm. The global alpha band rhythms have also been explored as a possible indicator of emotional states (Drennen and O'Reilly, 1986) and increased attention has been focused on the association of local alpha oscillations, including the occipital alpha oscillations, with cognitive operations (Klimesch, 1996, 1997). An interaction between anterior and posterior cortical circuits in the generation of human alpha rhythms has been supported by EEG coherence studies (Cantero et al., 1999, 2000; Srinivasan, 1999; Thatcher et al., 1986). This functional relationship could be anatomically supported by the superior longitudinal fasciculus traveling parallel to the midline (Cantero et al., 2002).

These findings suggest that the neural network for generating the EEG rhythm in both occipital and sensorimotor cortices might be similar and nonspecific. Studies using the frontal midline (mental) theta activities suggest that the prefrontal cortex including the anterior cingulate cortex might work as a generator of the state of internalized attention, which means manipulation of one's attentional focus during meditation (Aftanas and Golocheikine, 2001; Ishii et al., 1999; Sasaki et al., 1996). Thus, it is likely that the apparent positive correlation between the prefrontal activation and the increased idling rhythm at the sensorimotor or visual cortex can be due to the state of internalized attention facilitated by the rest condition with eyes closed.

EEG and PET methodology

Although the $H_2^{15}O$ tracer has much shorter time frame than the 18-fluoro-deoxyglucose tracer (20–30 min) and the results of $H_2^{15}O$ PET examinations directly depend on the acute cerebral state of activation during tracer injection (Schreckenberger et al., 2004), it is also true that the simultaneous PET and EEG recordings reflect EEG signals and cerebral blood flow changes which were temporally averaged over the span of 60 s. This diminished time resolution may be one of the limitations of the inter-modality correlation. However, it is likely that the EEG power should be stable during the PET scan time in the present study because we applied the simple repetitive movement tasks, in which the estimation of the task-related power change of the EEG was found to be useful (Andres et al., 1999; Gerloff et al., 1998; Toma et al., 2002).

Various types of EEG reference techniques may have different advantages and disadvantages for the EEG power estimation (Nunez et al., 1997). In the present study, we used the digitally linked earlobe reference. It is possible that the earlobe reference signal may contain the task-related EEG activity. However, none of our EEG electrodes (C3, C4, FC3, FC4, O1, O2) was located closer than ~6 cm to the reference electrodes, which may minimize the contribution of reference activation. To minimize the effect of common reference signal that is inevitably contaminated in the referenced EEG recording, we used the covariance analysis in which the task-related change of the EEG power and the task-related change of rCBF were compared.

Acknowledgments

References

Aftanas, L.I., Golocheikine, S.A., 2001. Human anterior and frontal midline theta and lower alpha reflect emotionally positive state and internalized attention: high-resolution EEG investigation of meditation. Neurosci. Lett. 310, 57–60.

Andres, F.G., Mima, T., Schulman, A.E., Dichgans, J., Hallett, M., Gerloff, C., 1999. Functional coupling of human cortical sensorimotor areas during bimanual skill acquisition. Brain 122, 855–870.

Arroyo, S., Lesser, R.P., Gordon, B., Uematsu, S., Jackson, D., Webber, R., 1993. Functional significance of the mu rhythm of human cortex: an electrophysiologic study with subdural electrodes. Electroencephalogr. Clin. Neurophysiol. 87, 76–87.

Bench, C.J., Friston, K.J., Brown, R.G., Scott, L.C., Frackowiak, R.S., Dolan, R.J., 1992. The anatomy of melancholia-focal abnormalities of cerebral blood flow in major depression. Psychol. Med. 22, 607–615.

Benoit, M., Koulibaly, P.M., Migneco, O., Darcourt, J., Pringuey, D.J., Robert, P.H., 2002. Brain perfusion in Alzheimer's disease with and without apathy: a SPECT study with statistical parametric mapping analysis. Psychiatry Res. 114, 103–111.

Berger, H., 1929. Uber das Elektrenkephalogramm des Menschen. Arch. Psychiatr. Nervenkrankh. 87, 527–570.

Berger, H., 1930. Uber das Elektrenkephalogramm des Menschen, 2nd report. J. Psychol. Neurol. (Leipzig) 40, 160–179.

Berger, H., 1932. Uber das Elektrenkephalogramm des Menschen, 4th report. Arch. Psychiatr. Nervenkrankh. 97, 6–26.

Bouyer, J.J., Montaron, M.F., Rougeul, A., 1981. Fast fronto-parietal rhythms during combined focused attentive behaviour and immobility in cat: cortical and thalamic localizations. Electroencephalogr. Clin. Neurophysiol. 51, 244–252.

Cantero, J.L., Atienza, M., Salas, R.M., Gomez, C.M., 1999. Alpha EEG coherence in different brain states: an electrophysiological index of the arousal level in human subjects. Neurosci. Lett. 271, 167–170.

Cantero, J.L., Atienza, M., Salas, R.M., 2000. State-modulation of cortico-cortical connections underlying normal EEG alpha variants. Physiol. Behav. 71, 107–115.

Cantero, J.L., Atienza, M., Salas, R.M., 2002. Human alpha oscillations in wakefulness, drowsiness period, and REM sleep: different electro-encephalographic phenomena within the alpha band. Neurophysiol. Clin. 32, 54–71.

Chen, R., Yaseen, Z., Cohen, L.G., Hallett, M., 1998. Time course of corticospinal excitability in reaction time and self-paced movements. Ann. Neurol. 44, 317–325.

Conway, B.A., Halliday, D.M., Farmer, S.F., Shahani, U., Maas, P., Weir, A.I., Rosenberg, J.R., 1995. Synchronization between motor cortex and spinal motoneuronal pool during the performance of a maintained motor task in man. J. Physiol. 489, 917–924.

Cooper, R., Winter, A.L., Crow, H.J., Walter, W.G., 1965. Comparison of subcortical, cortical and scalp activity using chronically indwelling electrodes in man. Electroencephalogr. Clin. Neurophysiol. 18, 217–228.

Crone, N.E., Miglioretti, D.L., Gordon, B., Sieracki, J.M., Wilson, M.T., Uematsu, S., Lesser, R.P., 1998. Functional mapping of human sensorimotor cortex with electrocorticographic spectral analysis. I. Alpha and beta event-related desynchronization. Brain 121, 2271–2299.

da Silva, F.H., van Lierop, T.H., Schrijer, C.F., van Leeuwen, W.S., 1973. Organization of thalamic and cortical alpha rhythms: spectra and coherences. Electroencephalogr. Clin. Neurophysiol. 35, 627–639.

Drennen, W.T., O'Reilly, B.K., 1986. Alpha enhancement: a comparison study of biofeedback, open focus training, and control procedures. Percept. Mot. Skills 62, 467–474.

Dum, R.P., Strick, P.L., 2002. Motor areas in the frontal lobe of the primate. Physiol. Behav. 77, 677–682.

Erecinska, M., Silver, I.A., 1989. ATP and brain function. J. Cereb. Blood Flow Metab. 9, 2–19.

Feng, C.M., Narayana, S., Lancaster, J.L., Jerabek, P.A., Arnow, T.L., Zhu, F., Tan, L.H., Fox, P.T., Gao, J.H., 2004. CBF changes during brain activation: fMRI vs. PET. NeuroImage 22, 443–446.

Friston, K.J., Frith, C.D., Liddle, P.F., Dolan, R.J., Lammertsma, A.A., Frackowiak, R.S., 1990. The relationship between global and local changes in PET scans. J. Cereb. Blood Flow Metab. 10, 458–466.

Friston, K.J., Frith, C.D., Liddle, P.F., Frackowiak, R.S., 1991. Comparing functional (PET) images: the assessment of significant change. J. Cereb. Blood Flow Metab. 11, 690–699.

Friston, K.J., Holmes, A.P., Worsley, K.J., Poline, J.B., Frith, C.D., Frackowiak, R.S., 1995. Statistical parametric maps in functional imaging: a general linear approach. Hum. Brain Mapp. 2, 189–210.

Gerloff, C., Richard, J., Hadley, J., Schulman, A.E., Honda, M., Hallett, M., 1998. Functional coupling and regional activation of human cortical motor areas during simple, internally paced and externally paced finger movements. Brain 121, 1513–1531.

Halliday, D.M., Rosenberg, J.R., Amjad, A.M., Breeze, P., Conway, B.A., Farmer, S.F., 1995. A framework for the analysis of mixed time series/point process data—theory and application to the study of physiological tremor, single motor unit discharges and electromyograms. Prog. Biophys. Mol. Biol. 64, 237–278.

Hari, R., Salmelin, R., 1997. Human cortical oscillations: a neuromagnetic view through the skull. Trends Neurosci. 20, 44–49.

Ingvar, D.H., Sjolund, B., Ardo, A., 1976. Correlation between dominant EEG frequency, cerebral oxygen uptake and blood flow. Electroence-phalogr. Clin. Neurophysiol. 41, 268–276.

Ishii, R., Shinosaki, K., Ukai, S., Inouye, T., Ishihara, T., Yoshimine, T., Hirabuki, N., Asada, H., Kihara, T., Robinson, S.E., Takeda, M., 1999. Medial prefrontal cortex generates frontal midline theta rhythm. NeuroReport 10, 675–679.

Klimesch, W., 1996. Memory processes, brain oscillations and EEG synchronization. Int. J. Psychophysiol. 24, 61–100.

Klimesch, W., 1997. EEG-alpha rhythms and memory processes. Int. J. Psychophysiol. 26, 319–340.

Klimesch, W., 1999. EEG alpha and theta oscillations reflect cognitive and memory performance: a review and analysis. Brain Res. Brain Res. Rev. 29, 169–195.

Kristiansen, K., Courtois, G., 1949. Rhythmic electrical activity from isolated cerebral cortex. Electroencephalogr. Clin. Neurophysiol. 3, 265–272.

Kuhlman, W.N., 1978. Functional topography of the human mu rhythm. Electroencephalogr. Clin. Neurophysiol. 44, 83–93.

Larson, C.L., Davidson, R.J., Abercrombie, H.C., Ward, R.T., Schaefer, S.M., Jackson, D.C., Holden, J.E., Perlman, S.B., 1998. Relations between PET-derived measures of thalamic glucose metabolism and EEG alpha power. Psychophysiology 35, 162–169.

Leuchter, A.F., Uijtdehaage, S.H., Cook, I.A., O'Hara, R., Mandelkern, M., 1999. Relationship between brain electrical activity and cortical perfusion in normal subjects. Psychiatry Res. 90, 125–140.

Lopes da Silva, F., 1991. Neural mechanisms underlying brain waves: from neural membranes to networks. Electroencephalogr. Clin. Neurophysiol. 79, 81–93.

Lopes da Silva, F.H., Vos, J.E., Mooibroek, J., Van Rotterdam, A., 1980. Relative contributions of intracortical and thalamo-cortical processes in the generation of alpha rhythms, revealed by partial coherence analysis. Electroencephalogr. Clin. Neurophysiol. 50, 449–456.

Lu, M.T., Preston, J.B., Strick, P.L., 1994. Interconnections between the prefrontal cortex and the premotor areas in the frontal lobe. J. Comp. Neurol. 341, 375–392.

Makeig, S., Westerfield, M., Jung, T.P., Enghoff, S., Townsend, J., Courchesne, E., Sejnowski, T.J., 2002. Dynamic brain sources of visual evoked responses. Science 295, 690–694.

Mattingley, J.B., Husain, M., Rorden, C., Kennard, C., Driver, J., 1998.

Motor role of human inferior parietal lobe revealed in unilateral neglect patients. Nature 392, 179–182.

Mima, T., Hallett, M., 1999. Electroencephalographic analysis of cortico-muscular coherence: reference effect, volume conduction and generator mechanism. Clin. Neurophysiol. 110, 1892–1899.

Mima, T., Sadato, N., Yazawa, S., Hanakawa, T., Fukuyama, H., Yonekura, Y., Shibasaki, H., 1999. Brain structures related to active and passive finger movements in man. Brain 122, 1989–1997.

Mima, T., Matsuoka, T., Hallett, M., 2000. Functional coupling of human right and left cortical motor areas demonstrated with partial coherence analysis. Neurosci. Lett. 287, 93–96.

Morecraft, R.J., Geula, C., Mesulam, M.M., 1992. Cytoarchitecture and neural afferents of orbitofrontal cortex in the brain of the monkey. J. Comp. Neurol. 323, 341–358.

Nagamine, T., Kajola, M., Salmelin, R., Shibasaki, H., Hari, R., 1996. Movement-related slow cortical magnetic fields and changes of spontaneous MEG- and EEG-brain rhythms. Electroencephalogr. Clin. Neurophysiol. 99, 274–286.

Nakamura, S., Sadato, N., Oohashi, T., Nishina, E., Fuwamoto, Y., Yonekura, Y., 1999. Analysis of music–brain interaction with simultaneous measurement of regional cerebral blood flow and electroencephalogram beta rhythm in human subjects. Neurosci. Lett. 275, 222–226.

Neuper, C., Pfurtscheller, G., 2001. Event-related dynamics of cortical rhythms: frequency-specific features and functional correlates. Int. J. Psychophysiol. 43, 41–58.

Niedermeyer, E., Lopes da Silva, F., 1987. Electroencephalography: Basic Principles, Clinical Applications, and Related Fields. Urban and Schwartzenberg.

Nofzinger, E.A., Price, J.C., Meltzer, C.C., Buysse, D.J., Villemagne, V.L., Miewald, J.M., Sembrat, R.C., Steppe, D.A., Kupfer, D.J., 2000. Towards a neurobiology of dysfunctional arousal in depression: the relationship between beta EEG power and regional cerebral glucose metabolism during NREM sleep. Psychiatry Res. 98, 71–91.

Nunez, P.L., Srinivasan, R., Westdorp, A.F., Wijesinghe, R.S., Tucker, D.M., Silberstein, R.B., Cadusch, P.J., 1997. EEG coherency. I: statistics, reference electrode, volume conduction, Laplacians, cortical imaging, and interpretation at multiple scales. Electroencephalogr. Clin. Neurophysiol. 103, 499–515.

Nunez, P.L., Wingeier, B.M., Silberstein, R.B., 2001. Spatial–temporal structures of human alpha rhythms: theory, microcurrent sources, multiscale measurements, and global binding of local networks. Hum. Brain Mapp. 13, 125–164.

Oakes, T.R., Pizzagalli, D.A., Hendrick, A.M., Horras, K.A., Larson, C.L., Abercrombie, H.C., Schaefer, S.M., Koger, J.V., Davidson, R.J., 2004. Functional coupling of simultaneous electrical and metabolic activity in the human brain. Hum. Brain Mapp. 21, 257–270.

Ohara, S., Nagamine, T., Ikeda, A., Kunieda, T., Matsumoto, R., Taki, W., Hashimoto, N., Baba, K., Mihara, T., Salenius, S., Shibasaki, H., 2000. Electrocorticogram–electromyogram coherence during isometric con-traction of hand muscle in human. Clin. Neurophysiol. 111, 2014–2024.

Paulson, O.B., Sharbrough, F.W., 1974. Physiologic and pathophysiologic relationship between the electroencephalogram and the regional cerebral blood flow. Acta Neurol. Scand. 50, 194–220.

Pfurtscheller, G., 1977. Graphical display and statistical evaluation of event-related desynchronization (ERD). Electroencephalogr. Clin. Neurophy-siol. 43, 757–760.

Pfurtscheller, G., 1981. Central beta rhythm during sensorimotor activities in man. Electroencephalogr. Clin. Neurophysiol. 51, 253–264.

Pfurtscheller, G., 1989. Functional topography during sensorimotor activation studied with event-related desynchronization mapping. J. Clin. Neurophysiol. 6, 75–84.

Pfurtscheller, G., 1992. Event-related synchronization (ERS): an electro-physiological correlate of cortical areas at rest. Electroencephalogr. Clin. Neurophysiol. 83, 62–69.

Pfurtscheller, G., Aranibar, A., 1977. Event-related cortical desynchroniza-tion detected by power measurements of scalp EEG. Electroencephalogr. Clin. Neurophysiol. 42, 817–826.

Pfurtscheller, G., Berghold, A., 1989. Patterns of cortical activation during planning of voluntary movement. Electroencephalogr. Clin. Neurophy-siol. 72, 250–258.

Pfurtscheller, G., Lopes da Silva, F.H., 1999. Event-related EEG/MEG synchronization and desynchronization: basic principles. Clin. Neuro-physiol. 110, 1842–1857.

Pfurtscheller, G., Stancak Jr., A., Neuper, C., 1996. Post-movement beta synchronization. A correlate of an idling motor area? Electroencepha-logr. Clin. Neurophysiol. 98, 281–293.

Pfurtscheller, G., Neuper, C., Krausz, G., 2000. Functional dissociation of lower and upper frequency mu rhythms in relation to voluntary limb movement. Clin. Neurophysiol. 111, 1873–1879.

Pineda, J.A., 2005. The functional significance of mu rhythms: translating "seeing" and "hearing" into "doing". Brain Res. Brain Res. Rev. 50, 57–68.

Raichle, M.E., 1987. Circulatory and metabolic correlates of brain function in normal humans. In: Mountcastle, V.B., Plum, F., Geiger, S.R. (Eds.), Handbook of Physiology Section 1: The Nervous System. Volume V. Higher Functions of the Brain. American Physiology Society, Bethesda, pp. 643–674.

Ramnani, N., Owen, A.M., 2004. Anterior prefrontal cortex: insights into function from anatomy and neuroimaging. Nat. Rev., Neurosci. 5, 184–194.

Rodriguez, E., George, N., Lachaux, J.P., Martinerie, J., Renault, B., Varela, F.J., 1999. Perception's shadow: long-distance synchronization of human brain activity. Nature 397, 430–433.

Rolls, E.T., 2004. The functions of the orbitofrontal cortex. Brain Cogn. 55, 11–29.

Rougeul, A., Bouyer, J.J., Dedet, L., Debray, O., 1979. Fast somato-parietal rhythms during combined focal attention and immobility in baboon and squirrel monkey. Electroencephalogr. Clin. Neurophysiol. 46, 310–319.

Rougeul-Buser, A., Buser, P., 1997. Rhythms in the alpha band in cats and their behavioural correlates. Int. J. Psychophysiol. 26, 191–203.

Sadato, N., Nakamura, S., Oohashi, T., Nishina, E., Fuwamoto, Y., Waki, A., Yonekura, Y., 1998. Neural networks for generation and suppression of alpha rhythm: a PET study. NeuroReport 9, 893–897.

Salenius, S., Salmelin, R., Neuper, C., Pfurtscheller, G., Hari, R., 1996. Human cortical 40 Hz rhythm is closely related to EMG rhythmicity. Neurosci. Lett. 213, 75–78.

Salmelin, R., Hari, R., 1994. Spatiotemporal characteristics of sensorimotor neuromagnetic rhythms related to thumb movement. Neuroscience 60, 537–550.

Salmelin, R., Hamalainen, M., Kajola, M., Hari, R., 1995. Functional segregation of movement-related rhythmic activity in the human brain. NeuroImage 2, 237–243.

Salmon, E., Collette, F., Degueldre, C., Lemaire, C., Franck, G., 2000. Voxel-based analysis of confounding effects of age and dementia severity on cerebral metabolism in Alzheimer's disease. Hum. Brain Mapp. 10, 39–48.

Sasaki, K., Nambu, A., Tsujimoto, T., Matsuzaki, R., Kyuhou, S., Gemba, H., 1996. Studies on integrative functions of the human frontal association cortex with MEG. Brain Res. Cogn. Brain Res. 5, 165–174.

Schreckenberger, M., Lange-Asschenfeld, C., Lochmann, M., Mann, K., Siessmeier, T., Buchholz, H.G., Bartenstein, P., Grunder, G., 2004. The thalamus as the generator and modulator of EEG alpha rhythm: a combined PET/EEG study with lorazepam challenge in humans. NeuroImage 22, 637–644.

Shimazu, H., Maier, M.A., Cerri, G., Kirkwood, P.A., Lemon, R.N., 2004. Macaque ventral premotor cortex exerts powerful facilitation of motor cortex outputs to upper limb motoneurons. J. Neurosci. 24, 1200–1211.

Sokoloff, L., 1977. Relation between physiological function and energy metabolism in the central nervous system. J. Neurochem. 29, 13–26.

Sokoloff, L., 1981. Relationships among local functional activity, energy metabolism, and blood flow in the central nervous system. Fed. Proc. 40, 2311–2316.

Srinivasan, R., 1999. Spatial structure of the human alpha rhythm: global correlation in adults and local correlation in children. Clin. Neurophysiol. 110, 1351–1362.

Staff, R.T., Venneri, A., Gemmell, H.G., Shanks, M.F., Pestell, S.J., Murray, A.D., 2000. HMPAO SPECT imaging of Alzheimer's disease patients with similar content-specific autobiographic delusion: comparison using statistical parametric mapping. J. Nucl. Med. 41, 1451–1455.

Steinmetz, H., Furst, G., Meyer, B.U., 1989. Craniocerebral topography within the international 10–20 system. Electroencephalogr. Clin. Neurophysiol. 72, 499–506.

Steriade, M., 1993. Cellular substrates of brain rhythms, In: Niedermeyer, E., Lopes da Silva, F.H. (Eds.), Electroencephalography: Basic Principles, Clinical Applications and Related Fields, 3rd ed. Williams and Wilkins, Baltimore, pp. 27–62.

Steriade, M., Llinas, R.R., 1988. The functional states of the thalamus and the associated neuronal interplay. Physiol. Rev. 68, 649–742.

Steriade, M., Gloor, P., Llinas, R.R., Lopes de Silva, F.H., Mesulam, M.M., 1990. Report of IFCN Committee on Basic Mechanisms. Basic mechanisms of cerebral rhythmic activities. Electroencephalogr. Clin. Neurophysiol. 76, 481–508.

Talairach, J., Tournoux, P., 1988. Co-planar Stereotaxic Atlas of the Human Brain. Thieme, Stuttgart.

Tallon-Baudry, C., Bertrand, O., 1999. Oscillatory gamma activity in humans and its role in object representation. Trends Cogn. Sci. 3, 151–162.

Thatcher, R.W., Krause, P.J., Hrybyk, M., 1986. Cortico-cortical associations and EEG coherence: a two-compartmental model. Electroencephalogr. Clin. Neurophysiol. 64, 123–143.

Tokuno, H., Nambu, A., 2000. Organization of nonprimary motor cortical inputs on pyramidal and nonpyramidal tract neurons of primary motor cortex: an electrophysiological study in the macaque monkey. Cereb. Cortex 10, 58–68.

Toma, K., Mima, T., Matsuoka, T., Gerloff, C., Ohnishi, T., Koshy, B., Andres, F., Hallett, M., 2002. Movement rate effect on activation and functional coupling of motor cortical areas. J. Neurophysiol. 88, 3377–3385.

Toro, C., Deuschl, G., Thatcher, R., Sato, S., Kufta, C., Hallett, M., 1994. Event-related desynchronization and movement-related cortical potentials on the ECoG and EEG. Electroencephalogr. Clin. Neurophysiol. 93, 380–389.

Vanni, S., Portin, K., Virsu, V., Hari, R., 1999. Mu rhythm modulation during changes of visual percepts. Neuroscience 91, 21–31.

Vijn, P.C., van Dijk, B.W., Spekreijse, H., 1991. Visual stimulation reduces EEG activity in man. Brain Res. 550, 49–53.

Wrobel, A., 2000. Beta activity: a carrier for visual attention. Acta Neurobiol. Exp. (Wars.) 60, 247–260.